HHS Public Access

Author manuscript

Brain Res. Author manuscript; available in PMC 2024 January 03.

Published in final edited form as:

Brain Res. 2022 January 01; 1774: 147721. doi:10.1016/j.brainres.2021.147721.

Peripherally administered cannabinoid receptor 2 (CB_2R) agonists lose anti-allodynic effects in TRPV1 knockout mice, while intrathecal administration leads to anti-allodynia and reduced GFAP, CCL2 and TRPV1 expression in the dorsal spinal cord and DRG

Jenny L. Wilkerson[a,c], **Lauren B. Alberti**[a], **Ganesh A. Thakur**[b], **Alexandros Makriyannis**[b], **Erin D. Milligan**[a,*]

[a]Department of Neurosciences, Health Sciences Center, School of Medicine, University of New Mexico, Albuquerque, NM 87131, USA

[b]Center for Drug Discovery, Northeastern University, Boston, MA 02115, USA

[c]Department of Pharmacodynamics, College of Pharmacy, University of Florida, Gainesville, FL, USA

Abstract

The transient receptor potential (TRP) superfamily of cation channels, of which the TRP vanilloid type 1 (TRPV1) receptor plays a critical role in inflammatory and neuropathic pain, is expressed on nociceptors and spinal cord dorsal horn neurons. TRPV1 is also expressed on spinal astrocytes and dorsal root ganglia (DRG) satellite cells. Agonists of the cannabinoid type 2 receptor (CB_2R) suppress allodynia, with some that can bind TRPV1. The neuroimmune C–C class chemokine-2 (CCL2) expressed on injured DRG nociceptor cell bodies, Schwann cells and spinal astrocytes, stimulates immune cell accumulation in DRG and spinal cord, a known critical element in chronic allodynia. The current report examined whether two CB_2R agonists, AM1710 and AM1241, previously shown to reverse light touch mechanical allodynia in rodent models of sciatic neuropathy, require TRPV1 activation that leads to receptor insensitivity resulting in reversal of allodynia. Global TRPV1 knockout (KO) mice with sciatic neuropathy given intrathecal or intraperitoneal AM1710 were examined for anti-allodynia followed by immunofluorescent microscopy analysis of lumbar spinal cord and DRG of astrocyte and CCL2 markers. Additionally, immunofluorescent analysis following intrathecal AM1710 and AM1241 in rat was performed.

*Corresponding author at: University of New Mexico, HSC, Dept. of Neurosciences, MSC08-4740, 1 University of New Mexico, Albuquerque, NM 87131, USA. Emilligan@salud.unm.edu (E.D. Milligan).

CRediT authorship contribution statement

Jenny L. Wilkerson: Conceptualization, Investigation, Formal analysis, Writing – original draft, Writing – review & editing. **Lauren B. Alberti:** Investigation. **Ganesh A. Thakur:** Resources. **Alexandros Makriyannis:** Resources. **Erin D. Milligan:** Conceptualization, Formal analysis, Writing – original draft, Writing – review & editing, Supervision, Funding acquisition.

Declaration of Competing Interest

The authors declare that they have no known competing financial interests or personal relationships that could have appeared to influence the work reported in this paper.

Appendix A. Supplementary data

Supplementary data to this article can be found online at https://doi.org/10.1016/j.brainres.2021.147721.

Data reveal that intrathecal AM1710 resulted in mouse anti-allodynia, reduced spinal astrocyte activation and CCL2 expression independent of TRPV1 gene deletion. Conversely, peripheral AM1710 in TRPV1-KO mice failed to reverse allodynia. In rat, intrathecal AM1710 and AM1241 reduced spinal and DRG TRPV1 expression, with CCL2-astrocyte and -microglial co-expression. These data support that CB_2R agonists can impact spinal and DRG TRPV1 expression critical for anti-allodynia.

Keywords

DRG; Mouse; Paraffin immunohistochemistry; Spectral analysis; Pain

1. Introduction

The endocannabinoid system is widely accepted to include the cannabinoid 1 receptor (CB_1R) and the cannabinoid 2 receptor (CB_2R). CB_1R is found on peripheral nociceptor cell bodies within the dorsal root ganglia (DRG) and on pre- and post-synaptic neurons in the superficial lamina of the dorsal horn spinal cord (Salio et al., 2002). CB_2R is found on peripheral immune cells and on glial cells such as satellite cells in the DRG (Chiocchetti et al., 2021; Svíženská et al., 2013; Carayon et al., 1998; Galiegue et al., 1995), and in the central nervous system (CNS) on astrocytes and microglia (Fernandez-Trapero et al., 2017; Núñez et al., 2008; Van Sickle et al., 2005; Galiegue et al., 1995). Activation of either the CB_1R or CB_2R has been extensively characterized to produce analgesia in numerous animal models of pathological pain (Donvito et al., 2018; Ahmed et al., 2010; Curto-Reyes et al., 2010; Romero-Sandoval et al., 2009). The CB_2R agonists AM1710 (Khanolkar et al., 2007) and AM1241 (Curto-Reyes et al., 2010; Ibrahim et al., 2003) are established to prevent and reverse neuropathy manifested as pathological sensitivity to light touch referred to as allodynia (Rahn et al., 2011; Wilkerson et al., 2012a; 2012b; Wilkerson et al., 2020), which is frequently observed in clinical neuropathic pain patients. Our group previously demonstrated that in rodent models of sciatic nerve injury resulting in allodynia, intrathecal (i.t.) AM1710 and AM1241 are capable of reversing allodynia, with simultaneous induction of a robust anti-inflammatory profile in both the spinal cord dorsal horn and corresponding DRG (Wilkerson et al., 2012a; 2012b; Wilkerson et al., 2020). However, while AM1241 and AM1710 have a ~36 fold and ~54-fold greater affinity for the CB_2R over the CB_1R, respectively (Khanolkar et al., 2007; Curto-Reyes et al., 2010; Ibrahim et al., 2003), non-specific actions at other receptors cannot be dismissed as a major contributing factor to the anti-allodynic effects of either peripherally or centrally administered CB_2R agonists.

In support of possible extra-CB_2R actions of AM1710 and AM1241, it has been found that endocannabinoids and CB_2R agonists can bind to the ligand-gated ion channel, transient receptor potential vanilloid type −1 (TRPV1) channel (Akopian et al., 2008). TRPV1 is widely characterized in the periphery on nociceptive (C and Aδ fiber) nerve terminals within the skin, and cell bodies within the DRG, and within the central nervous system (Akopian et al., 2008; Barbara et al., 2009). Further, there is accumulating evidence that within the CNS, TRPV1 is expressed on astrocytes (Roet et al., 2019; Mannari et al., 2013), and DRG satellite cells (Feldman-Goriachnik and Hanani, 2021; Gu et al., 2010; White et al., 2005).

When activated by noxious chemical stimulation, including capsaicin, the active ingredient in chili peppers, forskolin, or mustard seed oil (Bianchi et al., 2006), the TRPV1 channel is known to generate an inward flow of cations, such as Ca^{2+}(Fenwick et al., 2017; Himi et al., 2012; Caterina et al., 1997; Ma and Quirion, 2007). This influx of Ca^{2+} depolarizes neuronal signaling, leading to stimulus transduction ultimately producing the sensation of burning pain (Bianchi et al., 2006). Along similar lines, data show that when CB_2R agonists act as partial agonists at TRPV1, small inward currents and Ca2+ accumulation are generated. Consequently, threshold levels to produce action potentials in nociceptors are not generated (Akopian et al., 2008, 2009), suggesting CB_2R agonists act as weak TRPV1 agonists.

The existing data suggest the possibility that CB_2R agonists, as weak TRPV1 agonists, are capable of pharmacologically desensitizing the receptor without producing pain (Akopian et al., 2008; 2009). Indeed, it has been demonstrated *in vitro* that TRPV1 bound by CB_2R agonists results in reduced Ca2+ signaling events (Akopian et al., 2008). Additionally, a growing body of literature links the endocannabinoid system to TRPV1 activation, with cannabinoid agonists referred to as endovanilloids (De Petrocellis and Di Marzo, 2009; Van Der Stelt and Di Marzo, 2004; Starkus et al., 2019; Muller et al., 2018; Lowin and Straub, 2015; Patwardhan et al., 2006, Jeske et al., 2006; Fioravanti et al., 2008).

While allodynia from damage to axons of nociceptors is mediated by activated TRPV1, the expression of the neuroimmune chemokine, C–C class chemokine-2 (CCL2) formerly referred to as monocyte chemoattractant protein-1 (MCP-1), is elevated in DRG neuron cell bodies and further induces TRPV1 expression in DRG neurons (Kao et al., 2012). The well-characterized function of CCL2 in stimulating immune cell extravasation into the DRG and lumbar spinal cord (He et al., 2016; Gosselin et al., 2005) further supports its key role in exacerbating ongoing nociceptive processes, with these CCL2-mediated actions a critical element in chronic allodynia (Biber and Boddeke, 2014). Distinct from basal healthy conditions, pathological conditions trigger an increase CCL2 expression in spinal astrocytes (Zhang et al., 2017), DRG Schwann cells (Huang et al., 2020), and possibly DRG satellite cells (Lin et al., 2019), while reduced CCL2 is associated with attenuated allodynia (Hu et al., 2012; Van Steenwinckel et al., 2011; Thacker et al., 2009; Zhang et al., 2007).

The goal of the current report is to examine whether two previously studied CB_2R agonists, AM1710 and AM1241 characterized to reverse allodynia *in vivo,* require TRPV1 expression for anti-allodynic efficacy, and in parallel, impact spinal astrocyte activation, spinal and DRG CCL2 as well as TRPV1 expression. Additionally, we examined the spatial profile of TRPV1 on astrocytes and neurons under non-pathological and neuropathic conditions. Our prior reports demonstrate AM1710 reduces dorsal spinal and DRG proinflammatory interleukin-1β (IL-1β) expression and simultaneously elevates the potent anti-inflammatory cytokine interleukin-10 (IL-10) (Wilkerson et al., 2012a; 2012b; Wilkerson et al., 2020). The action of reducing proinflammatory cytokines while increasing anti-inflammatory cytokines acts as a powerful pain suppressant (Dengler et al., 2014; Vanderwall and Milligan, 2019; Milligan and Watkins, 2009). Therefore, in the current report using TRPV1 knockout (−/−) mice, we first sought to examine if TRPV1 is required for either peripheral or central *in vivo* efficacy of the CB_2R selective agonist AM1710. Microscopy analyses of DRG and dorsal spinal cord following TRPV1 immunohistochemical procedures were performed.

Additionally, astrocyte activation and cytokine expression were evaluated in the absence of TRPV1 under neuropathic conditions and after CB_2R agonist treatment. To complement work conducted in TRPV1 knockout (−/−) mice, the expression profile of TRPV1 was evaluated within rat spinal cord and DRG under neuropathic conditions and after intrathecal (i.t.) CB_2R agonist treatment. Because we wanted to examine if the expression profile of TRPV1 would be consistent across CB_2R agonists of different potency and receptor selectivity, we examined both AM1710 and AM1241, but continued characterizing AM1710 with regard to TRPV1 expression. To characterize the TRPV1 spatial profile with CCL2 on astrocytes and neurons, and to characterize the CCL2 spatial profile with IL10 on astrocytes and microglia, additional immunofluorescent microscopy was conducted. Together, these studies are aimed at gaining greater insight into the action of AM1710 and similar CB_2R compounds that may offer novel targets for future pain therapeutics.

2. Results

2.1. TRPV1(−/−) mice display similar allodynia profiles to (+/+), (+/−) littermates

The functional knockout of the TRPV1 (i.e., TRPV1(−/−)) produced no overt changes in the bilateral allodynia profiles obtained with CCI. Prior to surgical manipulation, all groups exhibited similar bilateral (ipsilateral and contralateral) baseline (BL) behavioral thresholds (ANOVA, $F_{(5,20)} = 3.418$; $p = 0.0215$, ANOVA, $F_{(5,20)} = 3.845$; $p = 0.0178$, respectively, for ipsilateral and contralateral paws). Unilateral CCI surgery produced significant, stable bilateral allodynia from Day 3 post CCI through Day 27 post CCI compared to sham-treated animals (ANOVA, $F_{(80,464)} = 7.353$; $p < 0.0001$, ANOVA, $F_{(80,464)} = 11.94$; $p < 0.0001$, respectively, for ipsilateral and contralateral paws) (Fig. 1 A,B). After Day 27 post-surgical manipulation, allodynia spontaneously resolved with hindpaw thresholds similar to sham levels. All groups of sham-operated mice exhibited thresholds similar to their baseline responses.

2.2. Intrathecal (i.t.) injection of AM1710 remains efficacious in reversing CCI-induced allodynia in TRPV1 (−/−) mice, with corresponding protein changes in lumbar spinal cord dorsal horn and DRG

The goal of this experiment is to determine whether the efficacy of i. t. AM1710 occurs independently from TRPV1. Before surgical manipulation, all experimental groups exhibited similar ipsilateral and contralateral BL hindpaw threshold responses (ANOVA, $F_{(11,55)} = 1.243$; $p = 0.2824$, ANOVA, $F_{(11,55)} = 2.045$; $p = 0.1404$, respectively). Sciatic CCI surgery produced significant bilateral allodynia at days 5 and 12 following injury compared to sham mice (ANOVA, $F_{(11,60)} = 194.1$; $p < 0.0001$, ANOVA, $F_{(11,60)} = 128.6$; $p < 0.0001$, respectively, for ipsilateral and contralateral paws). Regardless of the TRPV1 genotype, AM1710 (5 μg) maximally reversed CCI-induced allodynia at ~2 h after i.t. administration (ANOVA, $F_{(11,55)} = 57.97$; $p < 0.0001$, ANOVA, $F_{(11,55)} = 56.13$; $p < 0.0001$, respectively, for ipsilateral and contralateral paws). TRPV1 (+/+) and TRPV1 (−/−) ipsilateral and contralateral allodynia data are shown (Fig. 2 A,B), as well as allodynia from heterozygous TRPV1 (+/−) mice, (Supplemental Fig. 2 A,B).

Immunohistochemical analysis of ipsilateral spinal cord dorsal horn reveals GFAP immunoreactivity (IR) is dramatically increased regardless of TRPV1 genotype in CCI-induced neuropathic mice compared to sham-treated mice (ANOVA, $F_{(7,22)} = 9.427$; $p = 0.0002$) (Fig. 2 C). Similar effects are observed in the contralateral spinal cord (ANOVA, $F_{(7,22)} = 12.80$; $p < 0.0001$; Supplemental Fig. 2 C). Treatment with AM1710 decreased GFAP IR bilaterally to levels similar to non-neuropathic controls given either vehicle or AM1710. Representative immunofluorescent images represent ipsilateral dorsal horn of the spinal cord from TRPV1(+/+) mice with sham surgery and i.t. vehicle (Fig. 2 D), CCI surgery and i.t. vehicle (Fig. 2 E), or CCI surgery and i.t. AM1710 (Fig. 2 F) corresponding to the quantitative image analysis data.

Compared to non-neuropathic sham-operated mice, CCI induced a robust increase in CCL2 IR within the ipsilateral dorsal horn of the spinal cord in vehicle injected animals (ANOVA, $F_{(7,22)} = 14.03$; $p < 0.0001$, Fig. 2 G). Similar effects were observed in the contralateral spinal cord (ANOVA, $F_{(7,22)} = 31.84$; $p < 0.0001$; Supplemental Fig. 2 D). Conversely, i.t. administration of AM1710 decreased spinal cord dorsal horn CCL2 IR within 2 h of administration in TRPV1(+/+) and TRPV1 (−/−). Representative immunofluorescent images represent TRPV1(+/+) sham mice with i.t. vehicle (Fig. 2 H), CCI mice with i.t. vehicle (Fig. 2 I), or CCI mice with i.t. AM1710 (Fig. 2 J) that correspond to data examined by microscopy analysis.

In corresponding ipsilateral lumbar DRG, CCL2 IR is increased in CCI-induced neuropathic mice compared to sham-treated mice (ANOVA, $F_{(7,22)} = 22.01$; $p < 0.0001$; Fig. 4 K), with similar effects observed in the contralateral DRG (ANOVA, $F_{(7,22)} = 13.13$; $p < 0.0001$; Supplemental Fig. 2 E). In DRGs taken from behaviorally reversed CCI mice, AM1710 treatment suppressed CCL2 IR in DRGs from TRPV1 (+/+), but not from TRPV1(−/−) mice. Immunofluorescent images represent ipsilateral DRG from TRPV1(−/−) sham mice with i.t. vehicle (Fig. 2 L), CCI mice with i.t. vehicle (Fig. 2 M), or CCI mice with i.t. AM1710 (Fig. 2 N) that correspond to the quantitative image analysis data.

2.3. Reversal of allodynia from intrathecal (i.t.) AM1710 acts independently from CB_1R and TRPV1

In the absence of discernable involvement of TRPV1 in the anti-allodynic effects of i.t. AM1710, the possible role of CB_1R actions for AM1710 efficacy was examined. Before surgical manipulation, all experimental groups exhibited similar ipsilateral and contralateral BL hindpaw thresholds (ipsilateral: ANOVA, $F_{(2,8)} = 0.3391$; $p = 0.7311$; contralateral: ANOVA, $F_{(2,8)} = 0.03499$; $p = 0.9658$). In all groups of mice, CCI surgery produced similar bilateral allodynia at days 5 and 12 following injury (ipsilateral: ANOVA, $F_{(2,17)} = 0.6084$; $p = 0.5747$; contralateral: ANOVA, $F_{(2,17)} = 1.215$; $p = 0.3605$). Neuropathic TRPV1 (−/−) mice given an i.t. pretreatment of the selective CB_2R antagonist AM630 30-minutes prior to i.t. AM1710 revealed a lack of reversal from allodynia, as hindpaw thresholds were similar to i.t. vehicle-injected mice with CCI (ipsilateral: $p = 0.6939$, and contralateral: $p = 0.8998$), (Fig. 3 A, B). However, neuropathic TRPV1(−/−) mice given an i.t. pretreatment with the selective CB_1R antagonist AM251 thirty minutes prior to i.t. AM1710, fully reversed from

allodynia within ~2 hrs (ipsilateral: ANOVA, $F_{(2,8)} = 152.0$; $p = 0.0002$; contralateral: ANOVA, $F_{(2,8)} = 1091$; $p < 0.0001$).

2.4. Anti-allodynic efficacy of intraperitoneal (i.p.) AM1710 requires TRPV1

Given existing evidence demonstrates that CBRs are capable to desensitizing TRPV1 on nociceptors, an examination of intraperitoneal (i.p.) AM1710 was explored to determine whether its anti-allodynic effects were mediated by its actions on TRPV1. These studies utilized TRPV1(−/−) mice and applied CCI to induce allodynia. Before surgical manipulation, all experimental groups exhibited similar ipsilateral and contralateral BL thresholds (ipsilateral: ANOVA, $F_{(2,17)} = 1.772$; $p = 0.2195$; contralateral: ANOVA, $F_{(2,17)} = 2.908$; $p = 0.1010$). In all groups of mice, CCI surgery produced similar bilateral allodynia at days 5 and 12 following injury (ipsilateral: ANOVA, $F_{(2,35)} = 2.768$; $p = 0.0948$, contralateral ANOVA, $F_{(2,35)} = 1.927$; $p = 0.1799$). AM1710 given on Day 12 after surgery produced reversal of bilateral allodynia in TRPV1 (+/+) mice (ipsilateral: ANOVA, $F_{(2,17)} = 9.070$; $p = 0.0057$; contralateral: ANOVA, $F_{(2,17)} = 4.999$; $p = 0.0313$). While ipsilateral paw thresholds from TRPV1(+/−) mice displayed full reversal, contralateral hindpaw responses appeared to reflect partial reversal. However, hindpaw responses from TRPV1(−/−) mice given i.p. AM1710 revealed no change from allodynia; reversal from allodynia failed (Fig. 4 A, B).

2.5. Immunofluorescent analysis reveals intrathecal CB_2R agonist treatment decreases TRPV1 in neuropathic rat spinal cord and DRG

These studies additionally addressed the possible action of CB_2Rs on TRPV1 spinal expression following agonist administration. Our prior published reports extensively characterized anti-allodynia and neuroinflammatory cytokines in rat spinal cord and DRG following i.t AM1710 and AM1241. Therefore, in the current report, spinal cord and DRG from behaviorally-verified rats were examined for TRPV1 IR. Spinal cords from rats that underwent sham surgery and given i.t. AM1241 or AM1710 did not reveal altered TRPV1 immunoreactivity (IR) in the dorsal horn. However, in rats with CCI surgery, i.t. AM1241 significantly decreased bilateral spinal cord dorsal horn TRPV1 IR (ipsilateral: ANOVA, $F_{(3,11)} = 6.085$; $p = 0.0184$; contralateral: ANOVA, $F_{(3,11)} = 4.299$; $p = 0.0440$, (Fig. 5 A, B). Likewise, in rats with CCI surgery, i.t. AM1710 decreased bilateral TRPV1 IR (ipsilateral: ANOVA, $F_{(3,11)} = 4.416$; $p = 0.0413$; contralateral: ANOVA, $F_{(3,11)} = 3.354$; $p = 0.0760$) (Fig. 5 C, D).

An examination of bilateral L4-L5 DRG from previously behaviorally-verified rats revealed that compared to sham-operated rats given i.t. vehicle or AM1241, DRG from rats with CCI and treated with i. t. vehicle revealed increased TRPV1 IR in L4-L5 DRG (ipsilateral: ANOVA, $F_{(3,11)} = 16.14$; $p = 0.0009$; contralateral: ANOVA, $F_{(3,11)} = 4.390$; $p = 0.0419$), which was decreased with either i.t. AM1241 treatment (ipsilateral: ANOVA, $F_{(3,11)} = 6.13$; $p = 0.0181$; contralateral: ANOVA, $F_{(3,11)} = 6.971$; $p = 0.0127$) (Fig. 5 E, F), or i.t. AM1710 treatment (ipsilateral: ANOVA, $F_{(3,11)} = 10.85$; $p = 0.0034$; contralateral: ANOVA, $F_{(3,11)} = 10.90$; $p = 0.0033$), (Fig. 5 G, H).

2.6. Qualitative confocal images of TRPV1 immunoreactivity (IR) with astrocytes in spinal cord

To investigate the cellular location of TRPV1 in the dorsal horn of the spinal cord under sham and CCI conditions, immunohistochemical staining procedures followed by examination of immunofluorescent detection under microscopy was performed. Under basal conditions in sham rats, TRPV1 is found to be co-labeled with the astrocyte activation cell marker, GFAP, within the superficial lamina of the spinal cord dorsal horn (Fig. 6 A-D). Of note, clear co-labeling of TRPV1 and GFAP is observed near the medial white matter. Likewise, under neuropathic conditions induced by CCI (Fig. 6 E-H), co-labeling of TRPV1 and GFAP is also observed within the superficial lamina. Additionally, some co-labeling of TRPV1 with NF-H (neuron cell bodies and processes, cyan) is observed and is clustered around apparent neuronal cell bodies.

2.7. Qualitative confocal images of TRPV1 immunoreactivity (IR) with CCL2 in spinal cord and DRG

Given potential differences in peripheral vs. central involvement of TRPV1 with CB_2R anti-allodynic efficacy, examination of immunofluorescent of CCL2 was performed because CCL2 is characterized to increase TRPV1 expression. Immunofluorescent staining of TRPV1 co-labeled with CCL2 in the superficial lamina of the dorsal horn of the spinal cord in CCI-treated rats (Fig. 7 A-D) is observed, with co-labeling occurring with the astrocytic cell marker GFAP (cyan). Within deeper lamina 5, very clear co-labeling of TRPV1 and CCL2 on $GFAP^+$ cells is observed (Fig. 7 E-H). Within the superficial lamina, both TRPV1 and CCL2 are expressed on neurons (cyan) in a punctate pattern (Fig. 7 I-L). Within L5 DRG, very clear co-labeling of TRPV1 and CCL2 is observed on neuronal cell bodies, and smaller cell bodies surrounding larger cells (possibly satellite cells) (Fig. 7 M, N, O).

2.8. Qualitative confocal images of IL-10 with CCL2 or TRPV1 immunostaining in spinal cord

The spatial distribution of the anti-inflammatory cytokine, interleukin-10 (IL-10) with CCL2 or TRPV1 on astrocytes or microglia was examined in dorsal horn of the spinal cord from rats with CCI. IL-10 expression is characterized to increase in the spinal cord following AM1710, while also reducing CCL2 expression and astrocyte and microglial activation. Immunohistochemical fluorescent staining shows CCL2 is not extensively co-labeled with IL-10 in the superficial lamina of the dorsal horn of the spinal cord in CCI rats (Fig. 8 A-D). While speculative, CCL2 expression may be present on cells contained within the arachnoid/pia interface, as observed in the upper left corner of images A-D. However, clear co-labeling of CCL2 with GFAP (cyan) is present. A similar observation is found in deeper lamina. Within laminae V, co-labeling of IL-10 and CCL2 IR is observed on Iba-1 positive cells that identifies microglia and/or infiltrating *peri*-vascular myeloid cells (Fig. 8 E-H). Additionally, while IL-10 is expressed on cells with GFAP IR (astrocytes) under neuropathic conditions, no apparent co-labeling of IL10 with TRPV1 is observed. (Fig. 8. I-L).

3. Discussion

Here we characterize the length and severity of CCI-induced neuropathy in TRPV1 (+/+), (+/−), and (−/−) mice on a C57Bl/6 genetic background. As with our prior report (Wilkerson et al., 2020), clear bilateral allodynia persisted for approximately 30 days in wild type mice and in mice with TRPV1 genetic deletion in the current report. These data are the first demonstration evaluating the severity and duration of allodynia due to CCI in mice with TRPV1 (+/−) and (−/−) genetic backgrounds. These data further demonstrate that there are different underlying mechanisms whereby AM1710, a CB_2R agonist, reverses allodynia depending on the route of administration. Intrathecally, AM1710 is not reliant on actions of either CB_1R or TRPV1 and is selective for CB_2R. However, these anti-allodynic effects are reliant on the actions of TRPV1 when AM1710 is given by the systemic route, intraperitoneally. Of importance, systemically delivered compounds (i.e., i.p. route of administration) can undergo first pass metabolism, which can produce secondary bioactive metabolites (Kamble et al., 2018). First pass metabolism is avoided with i.t. administration and may account for some of the observed i.p. vs. i.t. differences including time course and TRPV1 involvement, described within this study. In both TRPV1 (+/+) and (−/−) neuropathic mice, i.t. administration of AM1710 markedly reduced GFAP and CCL2 IR within the dorsal horn of the spinal cord, further supporting that increased activation of spinal astrocytes following CCI play a role in allodynia and are activated by CCI independently from TRPV1 expression. Additionally, CCL2 is recognized as a critical spinal immune signaling chemokine driving the maintenance of allodynia and is likely derived from several cell types including from spinal nerve terminals of injured nociceptors and from infiltrating monocytes/macrophages. Interestingly, only neuropathic TRPV1(+/+) mice displayed a decrease in CCL2 within the DRG after AM1710 treatment, as CCL2 IR in TRPV1(−/−) tissues remained elevated after AM1710 treatment, suggesting that elevated CCL2 can persist despite allodynic reversal. The anti-allodynic action of the CB_2R agonist AM1710 does not require an interaction of CCL2 and TRPV1.

Although spinal TRPV1 appear dispensable in neuropathic rats, we found that TRPV1 IR is decreased after i.t. administration of two structurally different CB_2R agonists in both the dorsal horn of the spinal cord and DRG. We found co-labeling of TRPV1 on astrocytes, as identified by GFAP IR under both sham and neuropathic conditions. Further, in neuropathic rat spinal cord and DRG, co-labeling of TRPV1 and CCL2 in both astrocytes within the dorsal horn as well as satellite cells within the DRG was demonstrated. Conversely, although both TRPV1 and IL-10 are expressed by astrocytes within non-neuropathic rat dorsal horn spinal cord, their expression was not co-labeled on the same cell. It is possible that under pathological conditions such as that following peripheral neuropathy, the expression profile of TRPV1 and IL-10 on astrocytes changes.

The finding that the copy number of TRPV1 did not alter CCI-induced allodynia is likely specific to allodynia, and not to other experimental behavioral measures of pain. The observation that TRPV1 knockout mice display similar severity and duration of allodynia compared to their heterozygous and wild type littermates was predicted based on prior evidence (Bolcskei et al., 2005; Caterina et al., 2000). A notable exception to these findings appears to be found on day 7 after partial sciatic nerve ligation, where TRPV1 (−/−) mice

show a protective phenotype (Chen et al., 2009). TRPV1 (−/−) mice have also been reported to demonstrate lessened sensitivity to thermal hyperalgesia (Caterina et al., 2000).

Limited reports exist examining the spatial distribution of TRPV1 on astrocytes in the dorsal horn of the spinal cord in rodents (Doly et al., 2004). However, recent evidence from humans suggests that TRPV1 receptor expression on non-neuronal cells within the central nervous system is highest in astrocytes (Roet et al., 2019). Within the rodent central nervous system, it has also been demonstrated that perivascular astrocytes within the brain express TRPV1 (Mannari et al., 2013). Interestingly, CCL2 is expressed by vascular endothelial cells (Roblek et al., 2019; Khyzha et al., 2019), and CCL2 can augment TRPV1 expression in DRG neurons (Kao et al., 2012; Jung et al., 2008). Here, we show supporting evidence that under sham and neuropathic conditions, astrocytes and neurons within the superficial laminae of the dorsal horn of the spinal cord express TRPV1. In addition, results from the current report expand on our previous work which demonstrated that astrocytes in the deeper lamina express the anti-inflammatory cytokine IL-10 (Wilkerson et al., 2012a), as here, we show TRPV1 and IL-10 are co-expressed on astrocytes, but with a distinctly different spatial distribution.

The current report examined the anti-allodynia CB_2R selectivity of spinally administered AM1710 in neuropathic TRPV1(−/−) mice. The data unexpectedly demonstrate that TRPV1 is dispensable in order to achieve behavioral reversal of sciatic nerve injury-induced allodynia via i.t. AM1710. However, it is possible that underlying factors in the spinal cord driving neuropathy involve TRPV1 when it is present (e.g. in genetically intact mice), given our findings that TRPV1 IR was decreased after i.t. CB_2R treatment, and expressed on spinal astrocytes. Importantly, the data demonstrate that potential off-target effects of AM1710 at CB_1R or in a CB_2R-independent action are unlikely, given i.t. pre-treatment with AM630, a CB_2R antagonist blocked the effects of AM1710. Intrathecal pre-treatment with AM251, a CB_1R antagonist, however, did not alter the effects of spinal AM1710, supporting the existing *in vivo* evidence that intrathecally-delivered AM1710 acts in a CB_2R-specific manner (Deng et al., 2015; Wilkerson et al., 2012a; Wilkerson et al., 2020). In support of this CB_2R selectivity, the current report demonstrates that in behaviorally-verified TRPV1(−/−) mice, i.t. AM1710 resets spinal levels of elated GFAP and CCL2 IR to basal levels. In contrast, DRG examined from neuropathic TRPV1(−/−) mice demonstrated continued elevations in CCL2 IR following i.t. AM1710. Thus, it is possible that a bidirectional influence of CCL2 and TRPV1 within the DRG may occur in wild type mice, but that suppression of CCL2 in the DRG is not required for anti-allodynia.

One critical factor in controlling neuropathic pain may be increased levels of spinal CCL2. Importantly, CB_2R agonists, when delivered spinally, may participate in regulating CCL2 mediated pain. Indeed, these data support prior reports demonstrating increased CCL2 expression in both spinal cord pain-projection neurons and interneurons, astrocytes and DRG nociceptive neuronal cell bodies with CCI-induced neuropathy (White et al., 2005; Bhangoo et al., 2007; Jung et al., 2008; Hu et al., 2012; Jeon et al., 2009; Dansereau et al., 2008; Echeverry et al., 2011; Morin et al., 2007; Zhang et al., 2006, 2007). Other studies show that systemic (i.p.) administration of either AM1710 (Deng et al., 2015) or an enzyme inhibitor that increases endogenous activity of both CB_1R and CB_2R (Curry

et al., 2018) decrease pathological CCL2 elevations within the spinal cord and DRG from chemotherapy induced peripheral neuropathy. Here, we have extended these findings and show that in a surgical model of neuropathy, i.t. AM1710 dynamically regulates pathological expression of CCL2 in both the spinal cord and DRG in wildtype mice. It should be noted that the mechanics (i.e., specifically regarding the needle withdrawal from the intrathecal space) involved with performing intrathecal injections may have introduced the possibility that AM1710 was able to enter the peri-neural space around relevant DRGs (Wilkerson et al., 2012). Additionally, as CCL2 and the powerful anti-inflammatory cytokine IL-10 both involve microglia and infiltrating macrophages, further investigation into characterizing the role of these cell types that may underlie their importance, at least in part, on the anti-allodynic effects of AM1710 will provide important additional information in terms of potential druggable targets.

CB_2R agonists including AM1710 have been found to lack a discernable drug dependence and abuse liability profile as well as other untoward side effects (Li et al., 2018; Rahn et al., 2011; Kinsey et al., 2011). Indeed, AM1710 does not cross the blood brain barrier (Rahn et al., 2011). Combined, this profile of CB_2R agonists such as AM1710 support its potential as a promising first-generation small molecule drug to control pain, particularly in light of the current opioid epidemic, where few opioid-independent pain therapeutics are available. Anecdotal evidence and retrospective studies support that prescription opioid misuse can be a gateway for opioid addiction (Conroy and Hill, 2014, Mars et al., 2014) leading to long-term opioid exposure. It has been postulated that hyperkatifeia, or the state of enhanced sensitivity to emotional distress, is linked to long-term opioid misuse (Shurman et al., 2010). Opioid-related hyperkatifeia is further exacerbated by the current-day onslaught of unrelenting stress related to various facets of the COVID-19 pandemic, as recent evidence shows opioid misuse resulting in overdose has increased by ~38% in the United States during the first 12 months of the pandemic (Kuehn, 2021; Koob et al., 2020). Therefore, the need to develop opioid-independent pain therapeutics with diminished side effects as well as lessened abuse and dependence liability remains urgent. CB_2R agonists formulated to act in the periphery, and without the requirement of crossing the blood brain barrier to act in the central nervous system, may be promising effective non-opioid pain therapeutics.

The data show that the anti-allodynic effects of peripherally administered AM1710 are mediated by TRPV1. We speculate that TRPV1(−/−) mice may have compensatory mechanisms allowing CCL2 up-regulation in DRG under neuropathy. AM1710 may modulate peripheral TRPV1 function with possible actions within DRG, as prior reports have demonstrated that within the DRG, TRPV1 is upregulated in satellite cells under neuropathic conditions and modulates CCL2 actions (White et al., 2005). While other reports demonstrate that peripherally administered cannabinoids are capable of reversing neuropathy in animal models by binding to TRPV1 as partial agonists (Akopian et al., 2008; 2009), the current report demonstrates that TRPV1 is not a critical mediator of CCI-induced allodynia, and CB_2R suppression of CCL2 is not required for anti-allodynic efficacy. Crosstalk also exists within the TRPV family, and evidence demonstrates that activation of TRPV1 not only leads to its desensitization, but can also desensitize neighboring TRPVs (Lee et al., 2015; Takayama et al., 2015; Gordon-Shaag et al., 2008). The likelihood also exists that cannabinoid ligands are able to bind other TRP channels, such as TRPV2,

TRPA1 (Muller et al., 2018). Cannabinoid and TRP channels can be co-expressed within cells along the neural axis, raising the possibility that cannabinoid and TRP channels may form heterodimers. Therefore, it cannot be ruled out that other TRP receptors may also be critically involved in the current findings. Taken together, our results strongly support that bidirectional regulation of the endovanilloid and endocannabinoid systems occurs in key peripheral pain-pathway anatomical regions providing insight into developing novel pharmacological targets may yield promising non-opioid therapeutics for the treatment of neuropathic pain.

4. Materials and methods

4.1. Animals

A total of 110 pathogen-free adult male mice on a C57Bl/6 genetic background (24–30 g) were used in all experiments (Jackson Laboratories, Bar Harbor, ME). TRPV1(−/−), (+/−) and (+/+) mice were obtained from breeding TRPV1(−/−) mice on a C57Bl/6 genetic background (Jackson Laboratories, Bar Harbor, ME).

For rat spinal cord and DRG immunohistochemical studies tissues from previously published studies (Wilkerson et al., 2012a; 2012b) were used. Specifically, a total of 24 pathogen-free adult male Sprague Dawley rats (300–400 g; Harlan Labs, Madison, WI) were used in these previously published studies. Rats were double housed in a temperature- and light-controlled (12 h light/dark; lights on at 6:00 AM) environment, with standard rodent chow and water available ad libitum. Previously used methods, behavioral and immunohistochemical data obtained from the study of these rats (n = 3/group, sham surgery + vehicle injection, sham surgery + drug injection, CCI surgery + vehicle injection, CCI surgery + drug injection) are previously reported (Wilkerson et al., 2012a; 2012b).

All rodents were housed in a temperature and light-controlled (12 h light/dark; lights on at 6:00 AM) environment, with standard rodent chow and water available ad libitum. All procedures adhered to the guidelines of the Committee for Research and Ethical Issues of the International Association for the Study of Pain as well as ARRIVE Guidelines, (Kilkenny et al., 2010) and were approved by the Institutional Animal Care and Use Committee (IACUC) of the University of New Mexico Health Sciences Center.

4.2. Drugs

The CB_2R agonist, 3–1(1′,1′-Dimethylheptyl)-1-hydroxy-9-methoxy-6H-benzo[c]-chromene-6-one (AM1710) (Wilkerson et al., 2020; Wilkerson et al., 2012a; Rahn et al., 2011; Khanolkar et al., 2007) was used in these experiments and was synthesized by the Makriyannis laboratory. AM1710 was first dissolved in 100% ethanol and diluted in sterile water (Hospira Inc., Lake Forest, IL) for a final of concentration 1 mg/mL containing 5% ethanol. The selective CB_2R antagonist, 6-Iodo-2-methyl-1-[2-(4-morpholinyl)ethyl]-1H-indol-3-yl](4-methoxyphenyl) methanone, (AM630) and the selective CB_1R antagonist, N-(Piperidin-1-yl)-5-(4-iodophenyl)-1-(2,4-dichlorophenyl)-4-methyl-1H-pyrazole-3-carboxamide were purchased (cat # 1120, and 1117, respectively, Tocris Bioscience, Minneapolis, MN). As described for AM1710, both

AM630 and AM251 were first dissolved in 100% ethanol and diluted in sterile water (Hospira Inc, Lake Forest, IL) for a final concentration of 1 mg/ mL containing 5% ethanol. The vehicles of AM1710, AM630, and AM251 consisted of sterile water containing 5% ethanol, as described previously (Wilkerson et al., 2012a).

4.3. Behavioral assessment of allodynia

Baseline (BL) responses to light mechanical touch were assessed using the von Frey test after animals were habituated to the testing environment, as described elsewhere (Wilkerson et al., 2016; Wilkerson et al., 2020). Briefly, mice were placed on 2 mm-thick parallel bars, covered with a wire mesh screen, with spaces 1 mm apart and habituated for approximately 30 min for 4 days. Mice were unrestrained and were singly placed under an inverted wire mesh basket to allow for unrestricted air flow. All behavioral testing was performed during the first half of the light cycle in a sound, light, and temperature-controlled room. The von Frey test utilizes a series of calibrated monofilaments, (2.83 – 4.31 log stimulus intensity; North Coast Medical, Morgan Hills, CA) applied randomly to the left and right plantar surface of the hindpaw for 3 s. Lifting, licking or shaking the paw was considered a response. For all behavioral testing, threshold assessment was performed in a blinded fashion by J.L.W. All behavioral testing was conducted within the first four hours of the light cycle to decrease variance associated with circadian rhythm differences.

For absolute hindpaw-response threshold assessment, psychometric behavioral analysis was performed as previously described (Wilkerson et al., 2020; Treutwein and Strasburger, 1999) to compute the log stiffness that would have resulted in the 50% paw withdrawal rate. Briefly, thresholds were estimated by fitting a Gaussian integral psychometric function to the observed withdrawal rates for each of the tested von Frey hairs, using a maximum-likelihood fitting method. The total responses at each tested monofilament were used in the calculation of the absolute (50%) paw withdrawal threshold via the computer program PsychoFit (http://psych.colorado.edu/~lharvey; RRID: SCR_015381), as previously described (Wilkerson et al., 2020). This software fits a Gaussian integral psychometric function to the withdrawal responses for each of the monofilaments tested via a maximum-likelihood fitting method (Milligan et al., 2000). The log threshold values obtained from the Psychofit program were then used for subsequent statistical analyses.

4.4. Chronic constriction injury (CCI) surgery

Following BL behavioral assessment, the surgical procedure for chronic constriction injury (CCI) of the sciatic nerve was completed as previously described (Wilkerson et al., 2016; Wilkerson et al., 2020). Briefly, in isoflurane-(induction 5% vol. followed by 2.0% in oxygen) anesthetized mice, the mid- to lower back and the dorsal left thigh shaved and cleaned with 75% ethanol. Using aseptic procedures, the sciatic nerve was carefully isolated, and loosely ligated with 3 segments of 5–0 chromic gut sutures (Ethicon, Somerville, NJ). Sham surgery was identical to CCI surgery but without the loose nerve ligation. The overlying muscle was sutured closed with (1) 4–0 sterile silk suture (Ethicon, Somerville, NJ), and animals recovered from anesthesia within approximately 5 min. Animal placement into either CCI or sham surgical groups was randomly assigned. As previously described, use of chromic gut suture in the CCI model leads to bilateral mechanical allodynia,

with similar response thresholds observed between the ipsilateral and contralateral paws (Wilkerson et al., 2012; 2016; 2020).

4.5. Acute intrathecal (i.t.) injection

In mice with intrathecal (i.t.) injections, all drugs were administered via acute i.t. catheter placement as previously detailed (Wilkerson et al., 2020). Injections were performed via a lumbar puncture in between L5-L6. Briefly, an 'injection catheter' made from a 27-gauge needle with the plastic hub removed was fitted into polyethylene (PE) 20 tubing, and the needle portion of another 27-gauge needle was inserted at the other end, with the hub of this needle connected to a 10 μl Hamilton syringe, closely resembling the 'injection catheter' previously described (Milligan et al., 2006; 2005a; 2005b; Beutler et al., 2005). From previous publications doses of 5 μg AM1710 (Wilkerson et al., 2012a), 3 μg AM630 (Bilir et al., 2018; Gu et al., 2011), and 3 μg AM251 (Jiang et al., 2017; Curto-Reyes et al., 2010; Sink et al., 2009) were selected. Of note, the selected doses of AM251 and AM630 were previously found to be insufficient to alter pain-related or motor-related behaviors (Bilir et al., 2018; Ueda et al., 2014; Gu et al., 2011; Curto-Reyes et al., 2010; Sink et al., 2009). Drug or equivolume vehicle was drawn into the injection catheter, and the tip of the 27-gauge needle was gently inserted in between L5-L6. During this time, light leg twitching and a tail flick was typically observed indicating successful i.t. catheter placement. Drug or vehicle was injected during a 5 s interval, and intrathecal treatment was randomly assigned to animals. Upon completion of injection, the 27-gauge needle was removed. A 100% motor recovery rate was observed from this injection procedure.

4.6. Acute intraperitoneal injection

In CCI or sham mice an acute intraperitoneal (i.p.) injection of either AM1710 or equivolume vehicle was given. Prior reports (Rahn et al., 2011) indicate an effective dose of 25 mg/kg/ml (5 mg/kg) AM1710, which was administered in these studies.

4.7. Immunohistochemical procedures from CCI-treated mice and rats

Following behavioral assessment, animals were overdosed with an intraperitoneal injection sodium phenobarbital (Sleepaway, Fort Dodge Animal Health, Fort Dodge, IA), and transcardial perfusion with isotonic saline followed by 4% paraformaldehyde was performed. Whole vertebral columns with intact spinal cords (cervical 2 through sacral 1 spinal column segments) were removed, and underwent overnight fixation in 4% paraformaldehyde at 4 °C. This tissue collection approach ensured that all relevant anatomical components, including the cervical, thoracic, and lumbosacral spinal cord, DRG, and overlying meninges, were intact within the vertebral column, allowing important spatial relationships to remain for examining corresponding functional interactions at individual and specific spinal cord levels. All specimens underwent EDTA (Sigma Aldrich, St. Louis, MO) decalcification for approximately 2 weeks, and spinal cord sections were subsequently paraffin processed and embedded in Paraplast Plus Embedding Media (McCormick Scientific, St. Louis, MO) as previously described (Curry et al., 2018; Wilkerson et al., 2012a; 2012b). Adjacent tissue sections (7 μm) were mounted on Superfrost Plus slides (VWR, Radnor, PA), and allowed to adhere to slides overnight at 40 °C, followed by deparaffinization, and rehydration via descending alcohols to PBS (1X, pH 7.4). Sections

were then processed with microwave antigen retrieval procedures (citrate buffer pH 6.0, or tris-based buffer, pH 9.0; BioCare Medical, Concord, CA).

Slides were incubated with 5% normal donkey serum (NDS), in PBS (pH 7.4) for 2 h, followed by overnight primary antibody incubation in a humidity chamber at 3° C. Slides underwent secondary antibody incubation for 2 h in a humidity chamber at room temperature, rinsed in PBS, and then cover-slipped with Vectashield containing the nuclear stain 4′,6-diamidino-2-phenylindole (DAPI) (Vector Labs, Burlingame, CA). All antibody methods for glial fibrillary acidic protein (GFAP), ionized calcium binding adaptor molecule 1 (IBA-1), neurofilament H (NF-H) and interleukin-10 (IL-10) were as previously described (Curry et al., 2018; Wilkerson et al., 2012a; 2012b). For the detection of MCP-1/CCL2, an Armenian hamster anti-rat monoclonal antibody was used (clone 2H5, cat. # NB100–78196, Novus Biologicals, Littleton, CO), with a primary antibody dilution of 1:100, and detected with a Donkey anti-hamster FITC-tagged secondary antibody (Jackson Immunoresearch, West Grove, PA), (Curry et al., 2018). For neuronal nuclei (NEUN) staining, a mouse anti-NEUN monoclonal antibody was used (clone A60, cat # MAB377, Millipore, Billerica, MA) with a primary antibody dilution of 1:100 and detected with a donkey anti-mouse cy5 tagged secondary antibody (Jackson Immunoresearch, West Grove, PA), (Sarnat et al., 1998). For TRPV1 staining, a guinea pig anti-rat polyclonal antibody was used (cat # AB5566, Millipore, Billerica, MA), (Yu and Wang, 2011). Supplemental Fig. 1 shows qualitative images of TRPV1 staining achieved in spinal cord and DRG with this antibody. Rat tissues for immunohistochemical procedures (TRPV1 analysis and confocal microscopy) were paraffin embedded and from behaviorally verified animals that were previously published (Wilkerson et al., 2012a; 2012b).

4.8. Immunohistochemical spectral image analysis

All images of the spinal cord dorsal horn and DRGs were captured by a Nikon inverted fluorescent microscope (Melville, NY), at 20x magnification, with a Nuance Spectral Camera (Cambridge Research & Instrumentation, Woburn, MA), as previously described (Wilkerson et al., 2012a; 2012b). Briefly, utilizing the Nuance computer software, the fluorescent wavelength emission spectra range was initially determined for each fluorophore utilized in the detection of the primary antibody of interest (DAPI, 488 nm +/− 10 nm; FITC, 575 nm +/− 5 nm; Rhodamine Red 600 nm+/− 5 nm) by using a control slide with only a drop of the pure fluorophore. The fluorescent intensity threshold for each protein marker was determined by the user finding the most appropriate threshold that captures the specific FITC or Rhodamine Red staining for each protein marker within a tissue (e.g., dorsal horn spinal cord or DRG). Once the optimal level of fluorescent threshold was determined for a particular protein marker, this level was held consistent throughout all of the treatment groups for the image analysis within each protein marker of interest. These steps were followed by software conversion, thus allowing fluorescent wavelength intensity for each fluorophore to be converted to a numerical value.

Primary antibody staining procedures remained consistent to minimize intensity variations of each fluorophore (FITC or Rhodamine Red) used to detect the different primary antibodies of interest. To ensure that fluorophore binding was not impeded through possible

steric hindrance of other proximal fluorophores, sections were labeled for only one cellular marker of interest on a slide.

The average count of fluorescent emission intensity per second exposure, per mm^2 is the analyzed value that we report here. That is, fluorescent intensity average count/second/mm^2, which factors in the density as well as the intensity of the fluorophore detected. A total of 4 sections per animal (N = 3) were randomly selected and analyzed in this manner. By applying this method of data acquisition and analysis, experimenter bias is eliminated, yielding greater consistency and objectivity to fluorescent quantification (Wilkerson et al., 2012a; 2012b).

4.9. Confocal microscopy

All tissue processing, slicing, and procedures for immunohistochemistry were identical to that described above. However, in these studies, more than one primary antibody was used and examined under confocal microscopy. Therefore, after the first antibody staining procedure, the slides went through subsequent staining procedures. This took place over multiple days to account for the times needed for individual antibody incubation and staining. Confocal microscopy at 63 μm magnification was then performed on a Zeiss AxioObserver inverted LSM510 META confocal microscope utilizing Zen 2009 software (Carl Zeiss, AG, Oberkochen, Germany). Final images were generated from collapsed z-stacks comprising 17 images taken 0.393 μm apart on the z axis.

4.10. Data analysis

For behavioral statistical analysis in mice to assess the presence of allodynia, a 1-way ANOVA was used at BL, and a 2-way repeated measures ANOVA was used at timepoints following at indicated intervals from Day through day 40 after CCI/sham surgery. All IHC data analysis was performed using a one-way ANOVA. A p-value of <0.05 was considered statistically significant. The computer program GraphPad Prism version 4.03 (GraphPad Software Inc., San Diego, CA) was used in all statistical analyses. All data is expressed as mean +/− SEM. For post hoc analysis Tukey's test was performed.

Supplementary Material

Refer to Web version on PubMed Central for supplementary material.

Acknowledgements

This work was supported by the National Institute on alcohol Abuse and Alcoholism (NIAAA) R01 AA025967 (EDM), the National Institute on alcohol Abuse and Alcoholism (NIAAA) R21 AA023051 (EDM), the National institute on Drug Abuse (NIDA) R01 DA018156 (EDM), and the National Institute on alcohol Abuse and Alcoholism (NIAAA) P50 AA022534 (EDM) as well as funding from the Florida Consortium for Medical Marijuana Clinical Outcomes Research (JLW). The authors would like to thank Ms. Pamela Platero and Mr. Scott D. Contri for their technical assistance. The authors would like to thank Dr. James Wallace for his scholarly insights in tissue processing for immunohistochemistry and microscopy analysis.

Abbreviations:

BL Baseline

CB_1R	cannabinoid 1 receptor
CB_2R	cannabinoid 2 receptor
CCL2	C–C class chemokine 2
CCI	chronic constriction injury
CNS	central nervous system
DRG	dorsal root ganglia
GFAP	glial fibrillary acidic protein
HET	heterozygous
PE	polyethylene
IACUC	Institutional Animal Care and Use Committee
i.p.	intraperitoneal
i.t.	intrathecal
IF	immunofluorescent
IR	immunoreactivity
IBA-1	ionized calcium binding adaptor molecule 1
IL-10	interleukin-10
KO	knockout
MAPK	mitogen-activated kinases
MCP-1	monocyte chemoattractant protein-1
H (NF-H)	neurofilament
TRP	transient receptor potential
TRPV	transient receptor potential cation channel subfamily vanilloid
WT	wildtype

References

Ahmed MM, Rajpal S, Sweeney C, Gerovac TA, Allcock B, McChesney S, Patel AU, Tilghman JI, Miranpuri GS, Resnick DK, 2010. Cannabinoid subtype-2 receptors modulate the antihyperalgesic effect of WIN 55,212–2 in rats with neuropathic spinal cord injury pain. Spine J. 10 (12), 1049–1054. [PubMed: 20920894]

Akopian AN, Ruparel NB, Jeske NA, Patwardhan A, Hargreaves KM, 2009. Role of ionotropic cannabinoid receptors in peripheral antinociception and antihyperalgesia. Trends Pharmacol. Sci. 30 (2), 79–84. [PubMed: 19070372]

Akopian AN, Ruparel NB, Patwardhan A, Hargreaves KM, 2008. Cannabinoids desensitize capsaicin and mustard oil responses in sensory neurons via TRPA1 activation. J. Neurosci. 28 (5), 1064–1075. [PubMed: 18234885]

Barbara G, Alloui A, Nargeot J, Lory P, Eschalier A, Bourinet E, Chemin J, 2009. T-type calcium channel inhibition underlies the analgesic effects of the endogenous lipoamino acids. J. Neurosci. 29 (42), 13106–13114. [PubMed: 19846698]

Beutler AS, Banck MS, Walsh CE, Milligan ED, 2005. Intrathecal gene transger by adeno-associated virus for pain. Curr. Opin. Mol. Ther. 7, 431–439.

Biber K, Boddeke E, 2014. Neuronal CC chemokines: the distinct roles of CCL21 and CCL2 in neuropathic pain. Front. Cell. Neurosci. 8, 210. [PubMed: 25147499]

Bhangoo S, Ren D, Miller RJ, Henry KJ, Lineswala J, Hamdouchi C, Li B, Monahan PE, Chan DM, Ripsch MS, White FA, 2007. Delayed functional expression of neuronal chemokine receptors following focal nerve demyelination in the rat: a mechanism for the development of chronic sensitization of peripheral nociceptors. Mol. Pain 3:38. [PubMed: 18076762]

Bianchi BR, Lee C-H, Jarvis MF, El Kouhen R, Moreland RB, Faltynek CR, Puttfarcken PS, 2006. Modulation of human TRPV1 receptor activity by extracellular protons and host cell expression system. Eur. J. Pharmacol. 537 (1–3), 20–30. [PubMed: 16630609]

Bilir KA, Anli G, Ozkan E, Gunduz O, Ulugol A, 2018. Involvement of spinal cannabinoid receptors in the antipruritic effects of WIN 55,212–2, a cannabinoid receptor agonist. Clin. Exp. Dermatol. 43 (5), 553–558. [PubMed: 29424035]

Bolcskei K, Helyes Z, Szabo A, Sandor K, Elekes K, Nemeth J, Almasi R, Pinter E, Petho G, Szolcsanyi J, 2005. Investigation of the role of TRPV1 receptors in acute and chronic nociceptive processes using gene-deficient mice. Pain 117, 368–376. [PubMed: 16150543]

Carayon P, Marchand J, Dussossoy D, Derocq JM, Jbilo O, Bord A, Bouaboula M, Galiegue S, Mondiere P, Penarier G, Fur GL, Defrance T, Casellas P, 1998. Modulation and functional involvement of CB2 peripheral cannabinoid receptors during B-cell differentiation. Blood 92, 3605–3615. [PubMed: 9808554]

Caterina MJ, Leffler A, Malmberg AB, Martin WJ, Trafton J, Petersen-Zeitz KR, Koltzenburg M, Basbaum AI, Julius D, 2000. Impaired nociception and pain sensation in mice lacking the capsaicin receptor. Science 288 (5464), 306–313. [PubMed: 10764638]

Caterina MJ, Schumacher MA, Tominaga M, Rosen TA, Levine JD, Julius D, 1997. The capsaicin receptor: a heat-activated ion channel in the pain pathway. Nature 389 (6653), 816–824. [PubMed: 9349813]

Chen Y, Willcockson HH, Valtschanoff JG, 2009. Influence of the vanilloid receptor TRPV1 on the activation of spinal cord glia in mouse models of pain. Exp. Neurol. 220 (2), 383–390. [PubMed: 19815011]

Chiocchetti R, Rinnovati R, Tagliavia C, Stanzani A, Galiazzo G, Giancola F, Silva MD, Capodanno Y, Spadari A, 2021. Localisation of cannabinoid and cannabinoid-related receptors in the equine dorsal root ganglia. Equine Vet. J. 53 (3), 549–557. [PubMed: 32524649]

Conroy S, Hill D, 2014. Failure to identify or effectively manage prescription opioid dependence acted as a gateway to heroin use-buprenorphine/naloxone treatment and recovery in a surgical patient. BMJ Case Rep. 2014.

Curry ZA, Wilkerson JL, Bagdas D, Kyte SL, Patel N, Donvito G, Mustafa MA, Poklis JL, Niphakis MJ, Hsu K-L, Cravatt BF, Gewirtz DA, Damaj MI, Lichtman AH, 2018. Monoacylglycerol lipase inhibitors reverse paclitaxel-induced nociceptive behavior and proinflammatory markers in a mouse model of chemotherapy-induced neuropathy. J. Pharmacol. Exp. Ther. 366 (1), 169–183. [PubMed: 29540562]

Curto-Reyes V, Llames S, Hidalgo A, Menendez L, Baamonde A, 2010. Spinal and peripheral analgesic effects of the CB2 cannabinoid receptor agonist AM1241 in two models of bone cancer-induced pain. Br. J. Pharmacol. 160, 561–573. [PubMed: 20233215]

Dansereau MA, Gosselin RD, Pohl M, Pommier B, Mechighel P, Mauborgne A, Rostene W, Kitabgi P, Beaudet N, Sarret P, Melik-Parsadaniantz S, 2008. Spinal CCL2 pronociceptive action is no longer effective in CCR2 receptor antagonist-treated rats. J. Neurochem. 106:757–769. [PubMed: 18419759]

De Petrocellis L, Di Marzo V, 2009. Role of endocannabinoids and endovanilloids in Ca2+ signalling. Cell Calcium 45 (6), 611–624. [PubMed: 19356798]

Deng L, Guindon J, Cornett BL, Makriyannis A, Mackie K, Hohmann AG, 2015. Chronic cannabinoid receptor 2 activation reverses paclitaxel neuropathy without tolerance or cannabinoid receptor 1-dependent withdrawal. Biol. Psychiatry 77 (5), 475–487. [PubMed: 24853387]

Dengler EC, Alberti LA, Bowman BN, Kerwin AA, Wilkerson JL, Moezzi DR, Limanovich E, Wallace JA, Milligan ED, 2014. Improvement of spinal non-viral IL-10 gene delivery by D-mannose as a transgene adjuvant to control chronic neuropathic pain. J. Neuroinflammation 11, 92. [PubMed: 24884664]

Doly S, Fischer J, Salio C, Conrath M, 2004. The vanilloid receptor-1 is expressed in rat spinal dorsal horn astrocytes. Neurosci. Lett. 357 (2), 123–126. [PubMed: 15036590]

Donvito G, Nass SR, Wilkerson JL, Curry ZA, Schurman LD, Kinsey SG, Lichtman AH, 2018. The endogenous cannabinoid system: a budding source of targets for treating inflammatory and neuropathic pain. Neuropsychopharmacology 43 (1), 52–79. [PubMed: 28857069]

Echeverry S, Shi XQ, Rivest S, Zhang J, 2011. Peripheral nerve injury alters blood-spinal cord barrier functional and molecular integrity through a selective inflammatory pathway. J. Neurosci. 31 (30), 10819–10828. [PubMed: 21795534]

Feldman-Goriachnik R, Hanani M, 2021. How do neurons in sensory ganglia communicate with satellite glial cells? Brain Res. 1760, 147384. 10.1016/j.brainres.2021.147384.

Fenwick AJ, Fowler DK, Wu SW, Shaffer FJ, Lindberg JEM, Kinch DC, Peters JH, 2017. Direct anandamide activation of TRPV1 produces divergent calcium and current responses. Front. Mol. Neurosci. 10, 200. [PubMed: 28680392]

Fernandez-Trapero M, Espejo-Porras F, Rodriguez-Cueto C, Coates JR, Perez-Diaz C, de Lago E, Fernandez-Ruiz J, 2017. Upregulation of CB2 receptors in reactive astrocytes in canine degenerative myelopathy, a disease model of amyotrophic lateral sclerosis. Dis. Model. Mech. 10, 551–558. [PubMed: 28069688]

Fioravanti B, De Felice M, Stucky CL, Medler KA, Luo M-C, Gardell LR, Ibrahim M, Malan TP, Yamamura HI, Ossipov MH, King T, Lai J, Porreca F, Vanderah TW, 2008. Constitutive activity at the cannabinoid CB1 receptor is required for behavioral response to noxious chemical stimulation of TRPV1: antinociceptive actions of CB1 inverse agonists. J. Neurosci. 28 (45), 11593–11602. [PubMed: 18987195]

Galiegue S, Mary S, Marchand J, Dussossoy D, Carriere D, Carayon P, Bouaboula M, Shire D, Fur G, Casellas P, 1995. Expression of central and peripheral cannabinoid receptors in human immune tissues and leukocyte subpopulations. Eur. J. Biochem. 232 (1), 54–61. [PubMed: 7556170]

Gordon-Shaag A, Zagotta WN, Gordon SE, 2008. Mechanism of Ca(2+)-dependent desensitization in TRP channels. Channels (Austin) 2 (2), 125–129. [PubMed: 18849652]

Gosselin RD, Varela C, Banisadr G, Mechighel P, Rostene W, Kitabgi P, Melik-Parsadaniantz S, 2005. Constitutive expression of CCR2 chemokine receptor and inhibition by MCP-1/CCL2 of GABA-induced currents in spinal cord neurones. J. Neurochem. 95 (4), 1023–1034. [PubMed: 16150057]

Gu X, Mei F, Liu Y, Zhang R, Zhang J, Ma Z, 2011. Intrathecal administration of the cannabinoid 2 receptor agonist JWH015 can attenuate cancer pain and decrease mRNA expression of the 2B subunit of N-methyl-D-aspartic acid. Anesth. Analg. 113, 405–411. [PubMed: 21519057]

Gu Y, Chen Y, Zhang X, Li G-W, Wang C, Huang L-Y, 2010. Neuronal soma-satellite glial cell interactions in sensory ganglia and the participation of purinergic receptors. Neuron Glia Biol. 6 (1), 53–62. [PubMed: 20604979]

He M, Dong H, Huang Y, Lu S, Zhang S, Qian Y, Jin W, 2016. Astrocyte-Derived CCL2 is Associated with M1 Activation and Recruitment of Cultured Microglial Cells. Cell. Physiol. Biochem. 38 (3), 859–870. [PubMed: 26910882]

Himi N, Hamaguchi A, Hashimoto K, Koga T, Narita K, Miyamoto O, 2012. Calcium influx through the TRPV1 channel of endothelial cells (ECs) correlates with a stronger adhesion between monocytes and ECs. Adv. Med. Sci. 57 (2), 224–229. [PubMed: 23183769]

Hu J-H, Zheng X-Y, Yang J-P, Wang L-N, Ji F-H, 2012. Involvement of spinal monocyte chemoattractant protein-1 (MCP-1) in cancer-induced bone pain in rats. Neurosci. Lett. 517 (1), 60–63. [PubMed: 22531750]

Huang T, Fan Q, Wang Y, Cui Y, Wang Z, Yang L, Sun X, Wang Y, 2020. Schwann cell-derived CCL2 promotes the perineural invasion of cervical cancer. Front. Oncol. 10, 19. [PubMed: 32064233]

Ibrahim MM, Deng H, Zvonok A, Cockayne DA, Kwan J, Mata HP, Vanderah TW, Lai J, Porreca F, Makriyannis A, Malan TP, 2003. Activation of CB2 cannabinoid receptors by AM1241 inhibits experimental neuropathic pain: pain inhibition by receptors not present in the CNS. Proc. Natl. Acad. Sci. U. S. A. 100 (18), 10529–10533. [PubMed: 12917492]

Jeon S-M, Lee K-M, Cho H-J, 2009. Expression of monocyte chemoattractant protein-1 in rat dorsal root ganglia and spinal cord in experimental models of neuropathic pain. Brain Res. 1251, 103–111. [PubMed: 19059387]

Jeske NA, Patwardhan AM, Gamper N, Price TJ, Akopian AN, Hargreaves KM, 2006. Cannabinoid WIN 55,212–2 regulates TRPV1 phosphorylation in sensory neurons. J. Biol. Chem. 281 (43), 32879–32890. [PubMed: 16954222]

Jiang X, Yu M, Uy J, Fuller TW, Jones C, Shen B, Wang J, Roppolo JR, de Groat WC, Tai C, 2017. Role of cannabinoid receptor type 1 in tibial and pudendal neuromodulation of bladder overactivity in cats. Am. J. Physiol. Renal Physiol. 312 (3), F482–F488. [PubMed: 27927655]

Jung H, Toth PT, White FA, Miller RJ, 2008. Monocyte chemoattractant protein-1 functions as a neuromodulator in dorsal root ganglia neurons. J. Neurochem. 104, 254–263. [PubMed: 17944871]

Kamble SH, Sharma A, King TI, Leon F, McCurdy CR, Avery BA, 2018. Metabolite profiling and identification of enzymes responsible for the metabolism of mitragynine, the major alkaloid of Mitragyna speciosa (kratom). Xenobiotica 1, 1–31.

Kao D-J, Li AH, Chen J-C, Luo R-S, Chen Y-L, Lu J-C, Wang H-L, 2012. CC chemokine ligand 2 upregulates the current density and expression of TRPV1 channels and Nav1.8 sodium channels in dorsal root ganglion neurons. J. Neuroinflammation 9 (1). 10.1186/1742-2094-9-189.

Khanolkar AD, Lu D, Ibrahim M, Duclos RI Jr., Thakur GA, Malan TP Jr., Porreca F, Veerappan V, Tian X, George C, Parrish DA, Papahatjis DP, Makriyannis A, 2007. Cannabilactones: a novel class of CB2 selective agonists with peripheral analgesic activity. J. Med. Chem. 50, 6493–6500. [PubMed: 18038967]

Khyzha N, Khor M, DiStefano PV, Wang L, Matic L, Hedin U, Wilson MD, Maegdefessel L, Fish JE, 2019. Regulation of CCL2 expression in human vascular endothelial cells by a neighboring divergently transcribed long noncoding RNA. Proc. Natl. Acad. Sci. U. S. A. 116 (33), 16410–16419. [PubMed: 31350345]

Kilkenny C, Browne WJ, Cuthill IC, Emerson M, Altman DG, 2010. Improving bioscience research reporting: the ARRIVE guidelines for reporting animal research. PLoS Biol. 8, e1000412.

Kinsey SG, Mahadevan A, Zhao B, Sun H, Naidu PS, Razdan RK, Selley DE, Imad Damaj M, Lichtman AH, 2011. The CB2 cannabinoid receptor-selective agonist O-3223 reduces pain and inflammation without apparent cannabinoid behavioral effects. Neuropharmacology 60 (2–3), 244–251. [PubMed: 20849866]

Koob GF, Powell P, White A, 2020. Addiction as a Coping Response: Hyperkatifeia, Deaths of Despair, and COVID-19. Am. J. Psychiatry 177 (11), 1031–1037. [PubMed: 33135468]

Kuehn BM, 2021. Accelerated Overdose Deaths Linked With COVID-19. JAMA 325, 523.

Lee L-Y, Hsu C-C, Lin Y-J, Lin R-L, Khosravi M, 2015. Interaction between TRPA1 and TRPV1: Synergy on pulmonary sensory nerves. Pulm. Pharmacol. Ther. 35, 87–93. [PubMed: 26283426]

Li AL, Lin X, Dhopeshwarkar AS, Thomaz AC, Carey LM, Liu Y, Nikas SP, Makriyannis A, Mackie K, Hohmann AG, 2018. Cannabinoid CB2 agonist AM1710 differentially suppresses distinct pathological pain states and attenuates morphine tolerance and withdrawal. Mol. Pharmacol. 95, 155–168. [PubMed: 30504240]

Lin J, Liu F, Zhang YY, Song N, Liu MK, Fang XY, Liao DQ, Zhou C, Wang H, Shen JF, 2019. P2Y14 receptor is functionally expressed in satellite glial cells and mediates interleukin-1beta and chemokine CCL2 secretion. J. Cell. Physiol. 234, 21199–21210. [PubMed: 31032956]

Lowin T, Straub RH, 2015. Cannabinoid-based drugs targeting CB1 and TRPV1, the sympathetic nervous system, and arthritis. Arthritis Res. Ther. 17, 226. [PubMed: 26343051]

Ma W, Quirion R, 2007. Inflammatory mediators modulating the transient receptor potential vanilloid 1 receptor: therapeutic targets to treat inflammatory and neuropathic pain. Expert Opin. Ther. Targets 11 (3), 307–320. [PubMed: 17298290]

Mannari T, Morita S, Furube E, Tominaga M, Miyata S, 2013. Astrocytic TRPV1 ion channels detect blood-borne signals in the sensory circumventricular organs of adult mouse brains. Glia 61 (6), 957–971. [PubMed: 23468425]

Mars SG, Bourgois P, Karandinos G, Montero F, Ciccarone D, 2014. "Every 'never' I ever said came true": transitions from opioid pills to heroin injecting. Int. J. Drug Policy 25, 257–266. [PubMed: 24238956]

Martin D, Forsayeth JR, Maier SF, Johnson K, Chavez RA, Leinwand LA, Watkins LR, 2005a. Controlling pathological pain by adenovirally driven spinal production of the anti-inflammatory cytokine, Interleukin-10. Eur. J. Neurosci. 21: 2136–2148. [PubMed: 15869510]

Milligan ED, Sloane EM, Langer SJ, Cruz PE, Chacur M, Spataro L, Wieseler-Frank J, Hammack SE, Maier SF, Flotte TR, Forsayeth JR, Leinwand LA, Chavez RA, Watkins LR, 2005b. Controlling neuropathic pain by adeno-associated virus driven production of the anti-inflammatory cytokine, interleukin-10. Molecular Pain 1, 9–22. [PubMed: 15813997]

Milligan ED, Sloane EM, Langer SJ, Hughes TR, Jekich BM, Frank MG, Mahoney JH, Levkoff LH, Maier SF, Cruz PE, Flotte TR, Johnson KW, Mahoney MM, Chavez RA, Leinwand LA, Watkins LR, 2006. Repeated intrathecal injections of plasmid DNA encoding interleukin-10 produce prolonged reversal of neuropathic pain. Pain 126, 294–308. [PubMed: 16949747]

Milligan ED, Watkins LR, 2009. Pathological and protective roles of glia in chronic pain. Nat. Rev. Neurosci. 10 (1), 23–36. [PubMed: 19096368]

Morin N, Owolabi S, Harty M, Papa E, Tracyjr T, Shaw S, Kim M, Saab C, 2007. Neutrophils invade lumbar dorsal root ganglia after chronic constriction injury of the sciatic nerve. J. Neuroimmunol. 184 (1–2), 164–171. [PubMed: 17275921]

Muller C, Morales P, Reggio PH, 2018. Cannabinoid ligands targeting TRP channels. Front. Mol. Neurosci. 11, 487. [PubMed: 30697147]

Núñez E, Benito C, Tolón RM, Hillard CJ, Griffin WST, Romero J, 2008. Glial expression of cannabinoid CB(2) receptors and fatty acid amide hydrolase are beta amyloid-linked events in Down's syndrome. Neuroscience 151 (1), 104–110. [PubMed: 18068305]

Patwardhan AM, Jeske NA, Price TJ, Gamper N, Akopian AN, Hargreaves KM, 2006. The cannabinoid WIN 55,212–2 inhibits transient receptor potential vanilloid 1 (TRPV1) and evokes peripheral antihyperalgesia via calcineurin. Proc. Natl. Acad. Sci. U. S. A. 103 (30), 11393–11398. [PubMed: 16849427]

Rahn EJ, Thakur GA, Wood JAT, Zvonok AM, Makriyannis A, Hohmann AG, 2011. Pharmacological characterization of AM1710, a putative cannabinoid CB(2) agonist from the cannabilactone class: Antinociception without central nervous system side-effects. Pharmacol. Biochem. Behav. 98 (4), 493–502. [PubMed: 21382397]

Roblek M, Protsyuk D, Becker PF, Stefanescu C, Gorzelanny C, Glaus Garzon JF, Knopfova L, Heikenwalder M, Luckow B, Schneider SW, Borsig L, 2019. CCL2 is a vascular permeability factor inducing CCR2-dependent endothelial retraction during lung metastasis. Mol. Cancer Res. 17 (3), 783–793. [PubMed: 30552233]

Roet M, Jansen A, Hoogland G, Temel Y, Jahanshahi A, 2019. Endogenous TRPV1 expression in the human cingulate- and medial frontal gyrus. Brain Res. Bull. 152, 184–190. [PubMed: 31325598]

Romero-Sandoval EA, Horvath R, Landry RP, DeLeo JA, 2009. Cannabinoid receptor type 2 activation induces a microglial anti-inflammatory phenotype and reduces migration via MKP induction and ERK dephosphorylation. Mol. Pain 5:25. [PubMed: 19476641]

Salio C, Fischer J, Franzoni MF, Conrath M, 2002. Pre- and postsynaptic localizations of the CB1 cannabinoid receptor in the dorsal horn of the rat spinal cord. Neuroscience 110 (4), 755–764. [PubMed: 11934482]

Sarnat HB, Nochlin D, Born DE, 1998. Neuronal nuclear antigen (NeuN): a marker of neuronal maturation in early human fetal nervous system. Brain Dev 20, 88–94. [PubMed: 9545178]

Shurman J, Koob GF, Gutstein HB, 2010. Opioids, pain, the brain, and hyperkatifeia: a framework for the rational use of opioids for pain. Pain Med. 11 (7), 1092–1098. [PubMed: 20545871]

Sink KS, Segovia KN, Nunes EJ, Collins LE, Vemuri VK, Thakur G, Makriyannis A, Salamone JD, 2009. Intracerebroventricular administration of cannabinoid CB1 receptor antagonists AM251 and AM4113 fails to alter food-reinforced behavior in rats. Psychopharmacology 206 (2), 223–232. [PubMed: 19588124]

Starkus J, Jansen C, Shimoda LMN, Stokes AJ, Small-Howard AL, Turner H, 2019. Diverse TRPV1 responses to cannabinoids. Channels (Austin) 13 (1), 172–191. [PubMed: 31096838]

Svíženská IH, Brázda V, Klusáková I, Dubový P, 2013. Bilateral changes of cannabinoid receptor type 2 protein and mRNA in the dorsal root ganglia of a rat neuropathic pain model. J. Histochem. Cytochem. 61 (7), 529–547. [PubMed: 23657829]

Takayama Y, Uta D, Furue H, Tominaga M, 2015. Pain-enhancing mechanism through interaction between TRPV1 and anoctamin 1 in sensory neurons. Proc. Natl. Acad. Sci. U. S. A. 112 (16), 5213–5218. [PubMed: 25848051]

Thacker MA, Clark AK, Bishop T, Grist J, Yip PK, Moon LD, Thompson SW, Marchand F, McMahon SB, 2009. CCL2 is a key mediator of microglia activation in neuropathic pain states. Eur. J. Pain 13, 263–272. [PubMed: 18554968]

Treutwein B, Strasburger H, 1999. Fitting the psychometric function. Percept. Psychophys. 61 (1), 87–106. [PubMed: 10070202]

Ueda M, Iwasaki H, Wang S, Murata E, Poon KY, Mao J, Martyn JA, 2014. Cannabinoid receptor type 1 antagonist, AM251, attenuates mechanical allodynia and thermal hyperalgesia after burn injury. Anesthesiology 121, 1311–1319. [PubMed: 25188001]

van der Stelt M, Di Marzo V, 2004. Endovanilloids. Putative endogenous ligands of transient receptor potential vanilloid 1 channels. Eur. J. Biochem. 271 (10), 1827–1834. [PubMed: 15128293]

Vanderwall AG, Milligan ED, 2019. Cytokines in pain: harnessing endogenous anti-inflammatory signaling for improved pain management. Front. Immunol. 10, 3009. [PubMed: 31921220]

Van Sickle MD, Duncan M, Kingsley PJ, Mouihate A, Urbani P, Mackie K, Stella N, Makriyannis A, Piomelli D, Davison JS, Marnett LJ, Di Marzo V, Pittman QJ, Patel KD, Sharkey KA, 2005. Identification and functional characterization of brainstem cannabinoid CB2 receptors. Science 310 (5746), 329–332. [PubMed: 16224028]

Van Steenwinckel J, Reaux-Le Goazigo A, Pommier B, Mauborgne A, Dansereau M-A, Kitabgi P, Sarret P, Pohl M, Melik Parsadaniantz S, 2011. CCL2 released from neuronal synaptic vesicles in the spinal cord is a major mediator of local inflammation and pain after peripheral nerve injury. J. Neurosci. 31 (15), 5865–5875. [PubMed: 21490228]

White FA, Sun J, Waters SM, Ma C, Ren D, Ripsch M, Steflik J, Cortright DN, LaMotte RH, Miller RJ, 2005. Excitatory monocyte chemoattractant protein-1 signaling is up-regulated in sensory neurons after chronic compression of the dorsal root ganglion. Proc. Natl. Acad. Sci. U. S. A. 102 (39), 14092–14097. [PubMed: 16174730]

Wilkerson JL, Alberti LB, Kerwin AA, Ledent CA, Thakur GA, Makriyannis A, Milligan ED, 2020. Peripheral versus central mechanisms of the cannabinoid type 2 receptor agonist AM1710 in a mouse model of neuropathic pain. Brain Behav. 10 (12) 10.1002/brb3.v10.1210.1002/brb3.1850.

Wilkerson JL, Gentry KR, Dengler EC, Wallace JA, Kerwin AA, Armijo LM, Kuhn MN, Thakur GA, Makriyannis A, Milligan ED, 2012a. Intrathecal cannabilactone CB(2)R agonist, AM1710, controls pathological pain and restores basal cytokine levels. Pain 153, 1091–1106. [PubMed: 22425445]

Wilkerson JL, Gentry KR, Dengler EC, Wallace JA, Kerwin AA, Kuhn MN, Zvonok AM, Thakur GA, Makriyannis A, Milligan ED, 2012b. Immunofluorescent spectral analysis reveals the intrathecal cannabinoid agonist, AM1241, produces spinal anti-inflammatory cytokine responses in neuropathic rats exhibiting relief from allodynia. Brain Behav. 2 (2), 155–177. [PubMed: 22574283]

Wilkerson JL, Niphakis MJ, Grim TW, Mustafa MA, Abdullah RA, Poklis JL, Dewey WL, Akbarali H, Banks ML, Wise LE, Cravatt BF, Lichtman AH, 2016. The selective monoacylglycerol lipase inhibitor MJN110 produces opioid-sparing effects in a mouse neuropathic pain model. J. Pharmacol. Exp. Ther. 357 (1), 145–156. [PubMed: 26791602]

Yu SQ, Wang DH, 2011. Intrathecal injection of TRPV1 shRNA leads to increases in blood pressure in rats. Acta Physiol. (Oxf.) 203:139–147. [PubMed: 21518266]

Zhang J, De Koninck Y, 2006. Spatial and temporal relationship between monocyte chemoattractant protein-1 expression and spinal glial activation following peripheral nerve injury. J. Neurochem. 97, 772–783. [PubMed: 16524371]

Zhang Z-J, Jiang B-C, Gao Y-J, 2017. Chemokines in neuron-glial cell interaction and pathogenesis of neuropathic pain. Cell. Mol. Life Sci. 74 (18), 3275–3291. [PubMed: 28389721]

Zhang J, Shi XQ, Echeverry S, Mogil JS, De Koninck Y, Rivest S, 2007. Expression of CCR2 in both resident and bone marrow-derived microglia plays a critical role in neuropathic pain. J. Neurosci. 27 (45), 12396–12406. [PubMed: 17989304]

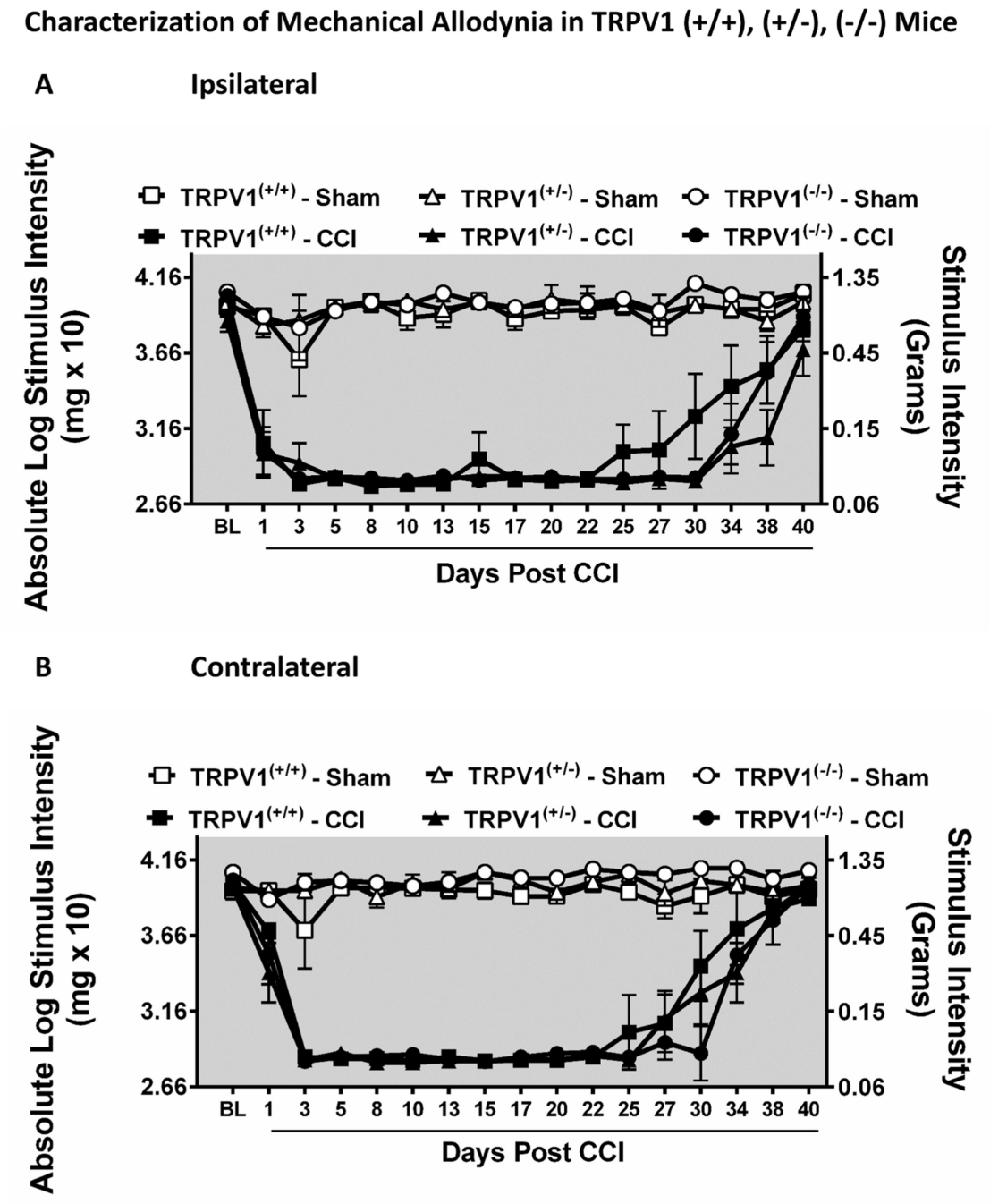

Fig. 1.

Characterization of magnitude and duration of bilateral allodynia in TRPV1(−/−) knockout (KO), (+/−) heterozygous (HET), and (+/+) wildtype (WT) mice. A, B, Mice develop and maintain CCI-induced ipsilateral and contralateral allodynia regardless of functional TRPV1 copy number. Before surgical manipulation, all experimental groups exhibited similar ipsilateral and contralateral hindpaw BL thresholds. Unilateral CCI surgery produced significant bilateral allodynia at Day 1 post CCI through Day 27 post CCI compared to sham mice. Data reflect mean ± SEM, n = 6 mice/group.

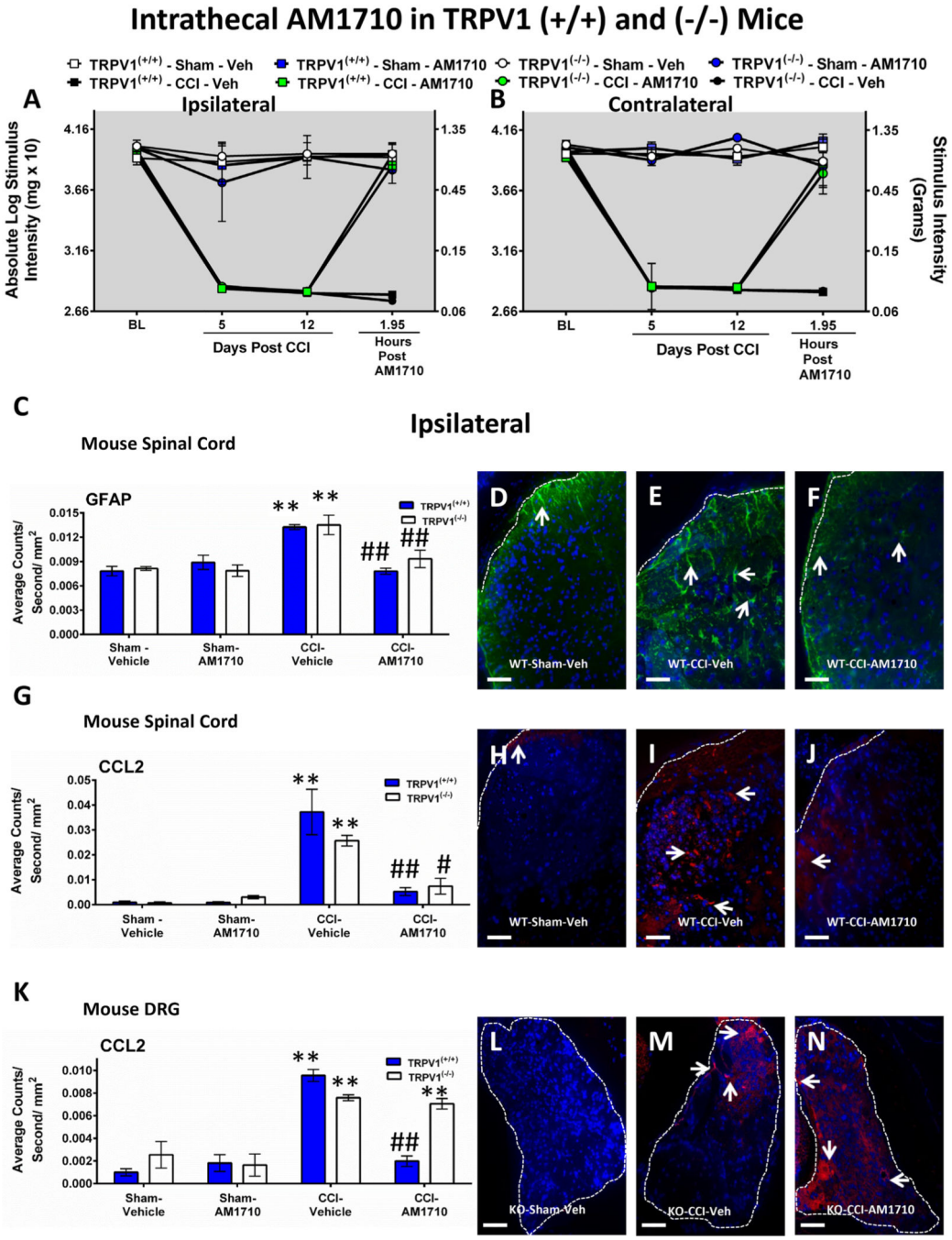

Fig. 2.

Intrathecal (i.t.) AM1710 reverses CCI-induced allodynia and modulates spinal GFAP, CCL2 in wild type and globally deleted TRPV1 knockout mice. A, B, AM1710 reverses CCI-induced allodynia independently of spinal TRPV1 actions. Unilateral CCI surgery produced significant bilateral allodynia in both TRPV1(+/+) wildtype (WT) and (−/−) knockout (KO) mice at Day 5 and 12 following unilateral injury. AM1710 (5 μg) maximally reversed CCI-induced allodynia in both TRPV1 (+/+) and (−/−) mice at ~2 h after i.t. administration. Sections of lumbar (L4-L6) dorsal horn spinal cord and corresponding

L4-L6 DRG taken from these behaviorally-verified mice were then analyzed. C, Semi-quantitative microscopy analysis of immunofluorescent immunoreactivity (IR) revealed GFAP expression in ipsilateral dorsal horn spinal cord was increased in both TRPV1(+/+) (striped bars) and TRPV1(−/−) (blue bars) CCI mice receiving i.t. vehicle compared to control sham mice given either i.t. vehicle or AM1710, while GFAP IR was significantly reduced in CCI neuropathic mice given i.t. AM1710. D, E, F, Representative spectral images at 20x magnification of GFAP IR labeling (green) with DAPI nuclear stain (blue) in ipsilateral dorsal horn spinal cord. White dashed lines indicate the border between spinal cord and intrathecal space. G, Irrespective of TRPV1 genetic background, compared to sham controls, CCL2 expression was increased in the ipsilateral dorsal horn spinal cord of CCI mice given i.t. vehicle. However, i.t. AM1710 in CCI mice robustly suppressed CCL2 IR. H, I, J, Representative spectral images at 20x magnification of CCL2 IR labeling (red) with DAPI nuclear stain (blue) in ipsilateral dorsal horn spinal cord. White dashed lines indicate the border between spinal cord and intrathecal space. K, Ipsilateral lumbar DRG demonstrate increased CCL2 expression from CCI mice that received i.t. vehicle compared to control sham mice. While CCL2 IR was decreased to sham levels in TRPV1(+/+) (striped bars), CCI mice given i.t. AM1710, TRPV1 (−/−) mice (blue bars) displayed continued elevated CCL2 IR in ipsilateral DRG. L, M, N, Representative spectral images at 20x magnification of CCL2 fluorescent labeling (red) with DAPI nuclear stain (blue) in ipsilateral DRG. The border around the DRG is indicated by white dashed lines. In all images the scale bar is equal to 50 μm. **$p < 0.01$, *$p < 0.05$ vs. Sham Vehicle-injected control, ##$p < 0.01$, #$p < 0.05$ vs. CCI Vehicle-injected control (Tukey's test), and results are mean ± S.E.M., n = 5–6 mice/group.

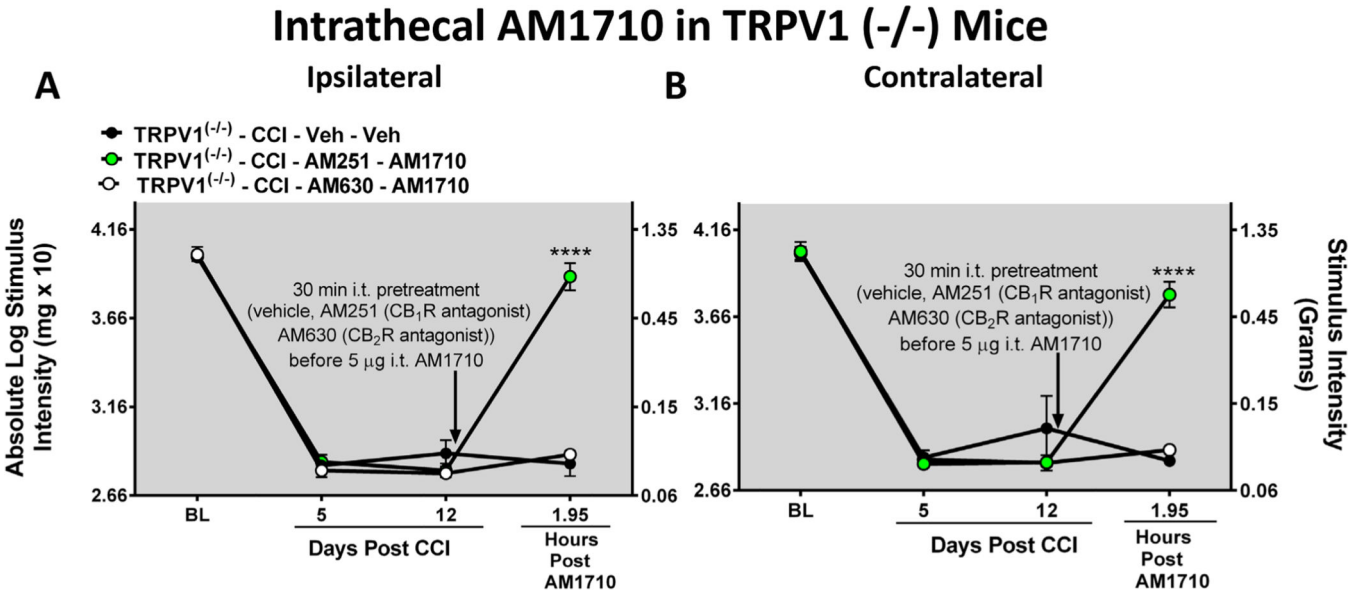

Fig. 3.

Intrathecal AM1710 reversal of allodynia requires CB_2R actions A, B, Intrathecal pre-treatment with the CB_2R selective antagonist AM630, but not the CB_1R antagonist AM251, blocks the bilateral reversal of allodynia by AM1710 in TRPV1(−/−) mice. ****$p < 0.0001$, vs. time matched CCI Vehicle-injected control (Tukey's test), and results are mean ± S.E.M, n = 3 mice/group.

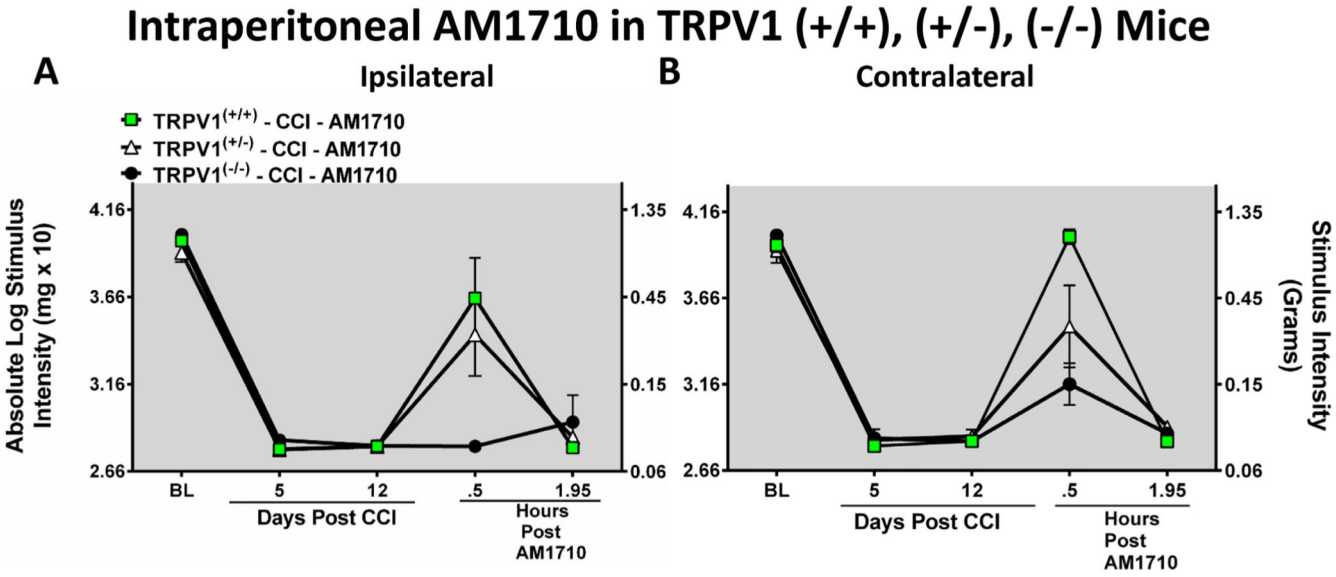

Fig. 4.

Intraperitoneal (i.p.) AM1710 reverses CCI-induced allodynia in TRPV1(+/+) and TRPV1(+/−), but not in TRPV(−/−) mice. A, B, In all groups of mice, unilateral CCI surgery produced similar bilateral allodynia at days 5 and 12 following injury. Thirty minutes following i.p. AM1710, full behavioral reversal of allodynia was observed in TRPV1 (+/+) and (+/−), but not (−/−) mice. Data reflect mean ± SEM, n = 6 mice/group.

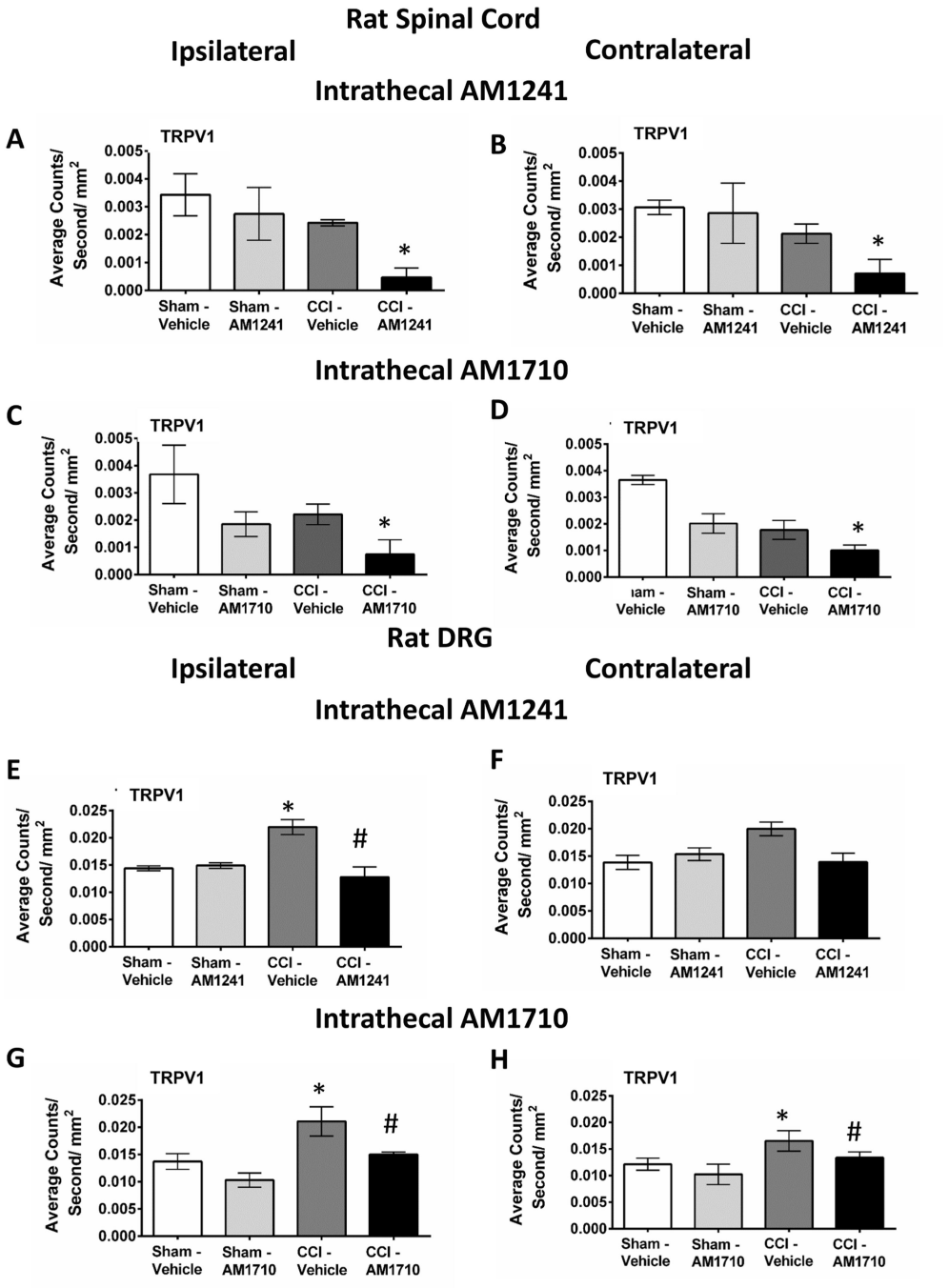

Fig. 5.

Intrathecal CB_2R agonist, AM1241 and AM1710 treatment decreases TRPV1 immunofluorescence in neuropathic rat spinal cord and DRG. A, B, In the dorsal horn of the spinal cord taken from unilateral CCI rats treated with intrathecal (i.t.) CB_2R agonist AM1241, TRPV1 IR is bilaterally decreased. C, D, TRPV1 IR is bilaterally decreased in the dorsal horn of the spinal cord taken from ipsilateral CCI rats given i.t. CB_2R agonist AM1710. E, F, In DRG, TRPV1 IR is increased following CCI-induced neuropathy and decreased with i.t. AM1241 in both ipsilateral and contralateral DRG. H, I, TRPV1 IR is

increased under CCI-induced neuropathy and decreased with i.t. AM1710 in both ipsilateral and contralateral DRG. *p < 0.05 vs. Sham vehicle-injected control, #p < 0.05 vs. CCI Vehicle-injected control (Tukey's test), and results are mean ± S.E.M., n = 3 rats/group.

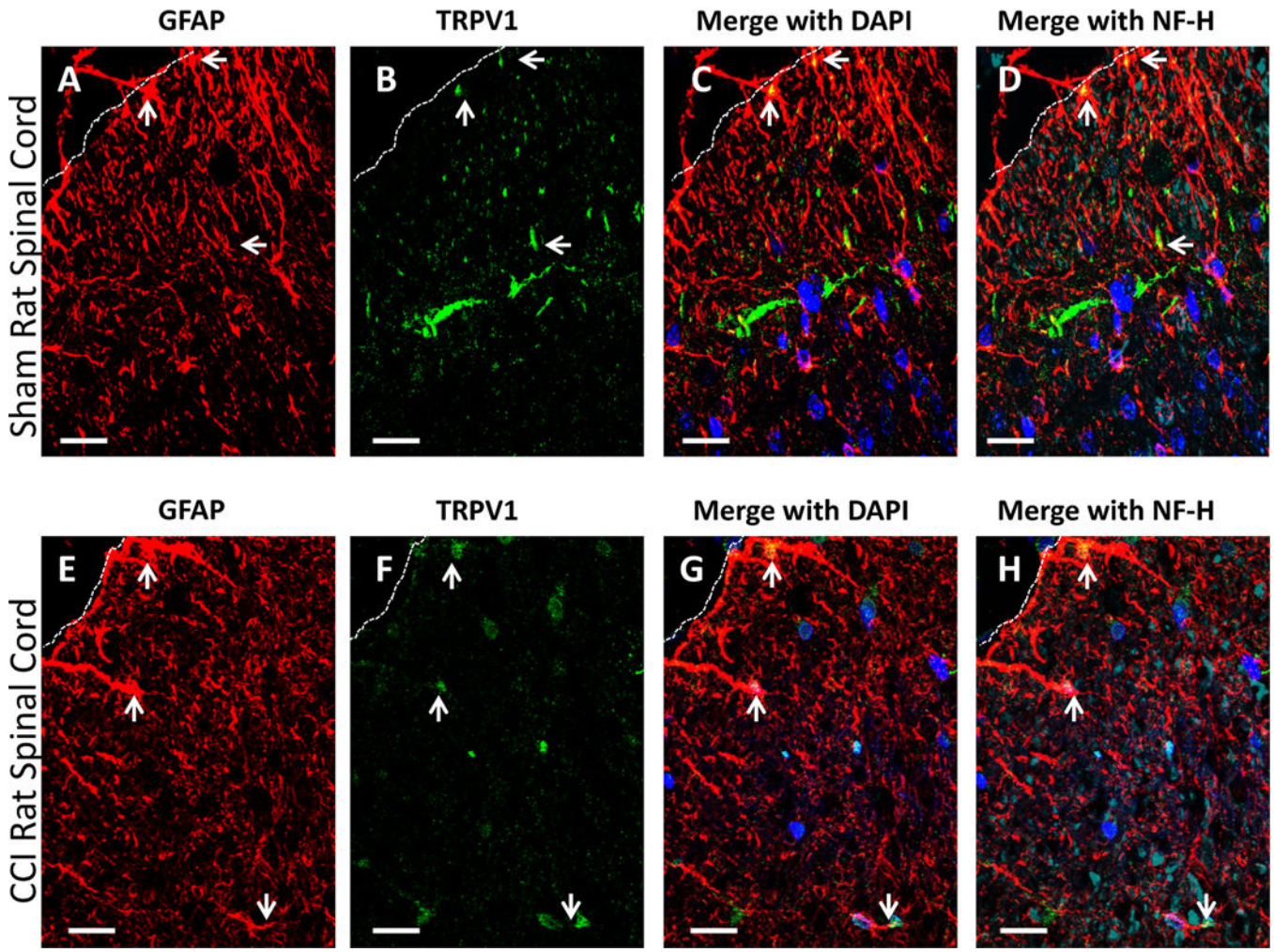

Fig. 6.

Qualitative confocal images of cellular immunofluorescent staining showing the spatial distribution of TRPV1 relative to astrocytes in spinal cord taken from sham and CCI-treated rats. (A-D) Spinal cord tissue from sham-treated rats. (E-H) Spinal cord tissue from CCI-treated rats. (A-D, E-H) Immunostaining of TRPV1 (green) in meninges and superficial laminae of the spinal cord and glial fibrillary acidic protein (GFAP) (red); co-labeled TRPV1 and GFAP appears yellow. 40,6-Diamidino-2-phenylindole (DAPI) nuclear labeling is blue, and neurofilament-H (NF-H) is cyan. White dashed lines indicate the border between spinal cord and intrathecal space. Arrows indicate GFAP and TRPV1, and co-expression in the superficial laminae. In all images the scale bar is equal to 20 um.

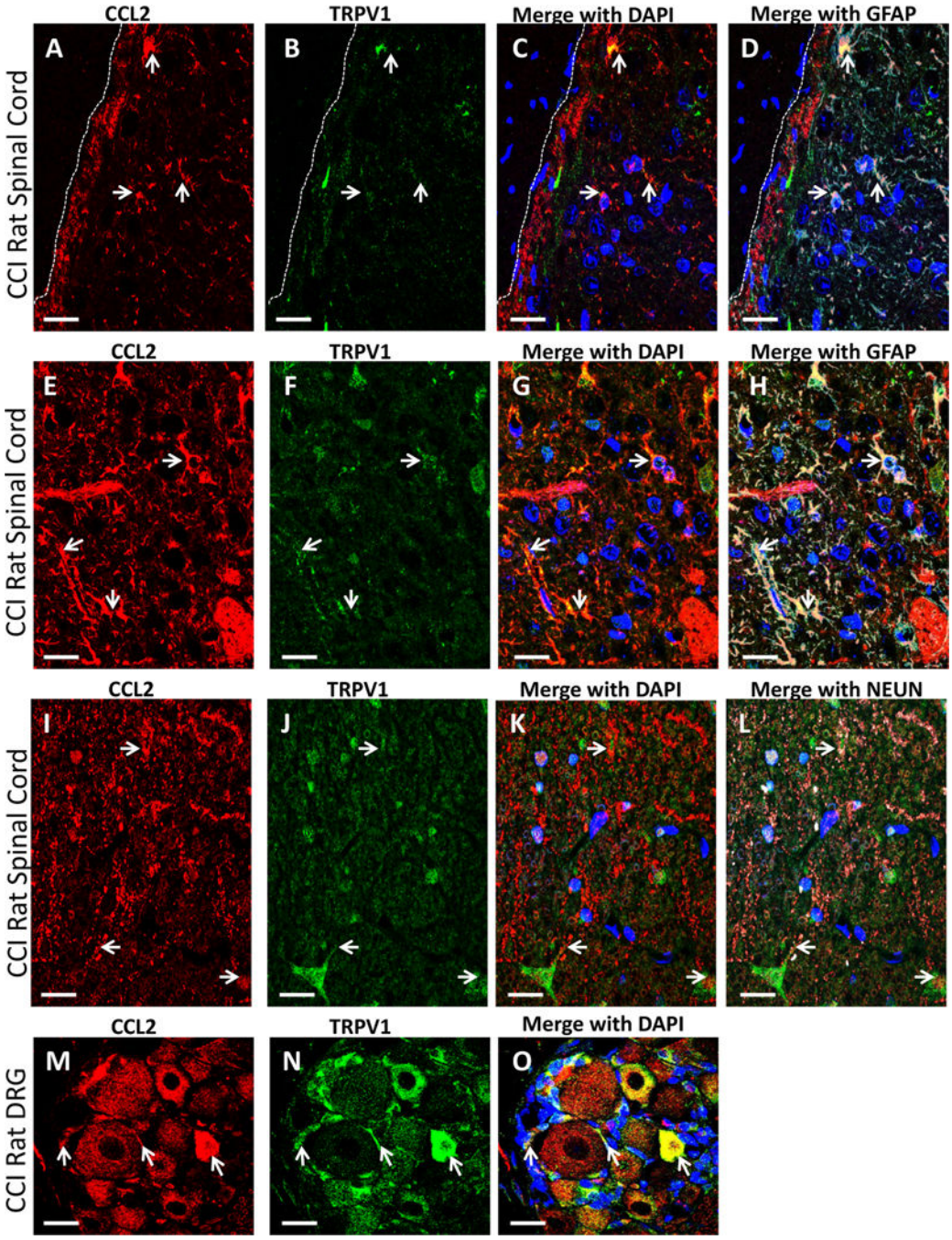

Fig. 7.

Qualitative confocal images of cellular IF staining of TRPV1, CCL2, and GFAP in rat lumbar dorsal horn spinal cord and DRG. (A-L) Spinal cord tissue from neuropathic rats. (A-D) Immunostaining of CCL2 (red), TRPV1 (green) in superficial laminae of the spinal cord dorsal horn, with co-labeling of IR (yellow), often on GFAP positive astrocytes (cyan). White arrows indicate regions of overlap with CCL2, TRPV1 and GFAP. DAPI nuclear labeling is also shown (blue). White dashed lines indicate the border between spinal cord and intrathecal space. (E-H) Deeper laminae of the dorsal horn of the spinal cord revealing

IR of CCL2 (red) and TRPV1 (green) in with co-labeled (yellow) regions on GFAP positive astrocytes (cyan), as indicated with arrows. DAPI nuclear labeling is also shown (blue). (I-L) Deeper laminae of the dorsal horn of the spinal cord revealing IR of CCL2 (red) and TRPV1 (green) with neurons stained with Neun (cyan). DAPI nuclear labeling is shown (blue). Arrows indicate neurons that express both proteins. (M− O) DRG IR of CCL2 (red), and TRPV1 (green) in neuropathic rats revealing co-labeled staining (yellow) on neuronal cell bodies (white arrows) and small non-neuronal (possibly satellite cells; white arrows). DAPI nuclear labeling is shown (blue). In all images the scale bar is equal to 20 um.

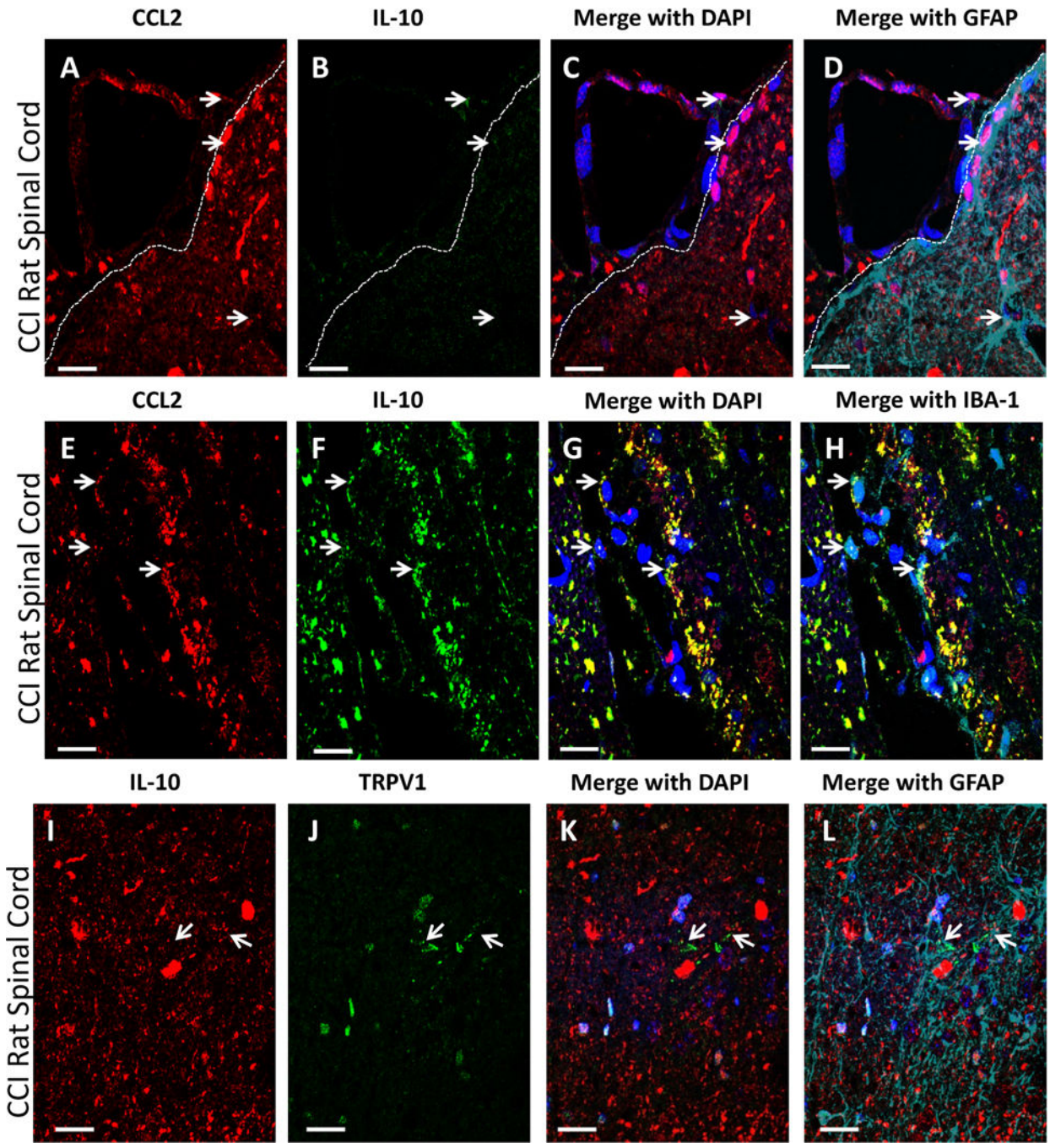

Fig. 8.

Qualitative confocal images of cellular immunofluorescent staining of CCL2 and IL-10 in GFAP IR astrocytes. (A-L) Superficial spinal cord tissue from CCI-treated rats. (A-D), In meninges and superficial laminae of the spinal cord dorsal horn, IR of CCL2 (red) and IL-10 (green) are *not* co-labeled. GFAP+ (cyan) cells do not appear to express IL-10 IR. DAPI nuclear labeling is blue. Arrows indicate IL-10 and CCL2 IR. White dashed lines indicate the border between spinal cord and intrathecal space. (E-H) In deeper laminae of the spinal cord dorsal horn (LV), IR of CCL2 (red) and IL-10 (green) are co-labeled yellow,

that appear to be abundantly present on IBA-1^{+} (microglia/infiltrating macrophage; cyan) cells, as indicated with white arrows. DAPI nuclear labeling is shown (blue). (I-L) TRPV1 (green) and IL-10 (red) are not readily co-labeled, although both are expressed by GFAP (cyan)-positive cells, with DAPI nuclear labeling (blue) in the spinal cord dorsal horn of a neuropathic rat. Arrows indicate astrocytes with separate IL-10 and TRPV1 labeling. In all images the scale bar is equal to 20 um.